A novel biomimetic nanofibrous cardiac tissue engineering scaffold with adjustable mechanical and electrical properties based on poly(glycerol sebacate) and polyaniline

Zebin Wu [a], Qiao Li [a,b], Lizhen Wang [a,*], Yang Zhang [a], Wei Liu [c], Shudong Zhao [a], Xuezheng Geng [a], Yubo Fan [a,b,**]

[a] *Key Laboratory for Biomechanics and Mechanobiology of Ministry of Education, Beijing Advanced Innovation Centre for Biomedical Engineering, School of Biological Science and Medical Engineering, Beihang University, Beijing 100083, China*
[b] *School of Engineering Medicine, Beihang University, Beijing 100083, China*
[c] *Department of Cardiology, Beijing Jishuitan Hospital, Capital Medical University, Beijing 100035, China*

ARTICLE INFO

ABSTRACT

Biomaterial tissue engineering scaffolds play a critical role in providing mechanical support, promoting cells growth and proliferation. However, due to the insulation and inappropriate stiffness of most biomaterials, there is an unmet need to engineer a biomimetic nanofibrous cardiac tissue engineering scaffold with tailorable mechanical and electrical properties. Here, we demonstrate for the first time the feasibility to generate a novel type of biocompatible fibrous scaffolds by blending elastic poly(glycerol sebacate) (PGS) and conductive polyaniline (PANI) with the help of a nontoxic carrier polymer, poly (vinyl alcohol) (PVA). Aligned and random PGS/PANI scaffolds are successfully obtained after electrospinning, cross-linking, water and ethanol wash. Incorporating of different concentrations of PANI into PGS fibers, the fibrous sheets show enhanced conductivity and slower degradation rates while maintaining the favorable hemocompatibility. The elastic modulus of the PGS/PANI scaffolds is in the range of 0.65–2.18 MPa under wet conditions, which is similar to that of natural myocardium. All of these fibrous mats show good cell viability and were able to promote adhesion and proliferation of H9c2 cells. Furthermore, the in vivo host responses of both random and aligned scaffolds confirm their good biocompatibility. Therefore, these PGS/PANI scaffolds have great potential for cardiac tissue engineering.

1. Introduction

Numerous patients suffer from myocardial infarction (MI) around the world, which causes high probability of heart failure and even death. Current strategies for MI such as medicine, percutaneous coronary intervention (PCI), heart transplantation and etc. are not satisfactory due to the complications of surgery, shortage of enough donor hearts and limited regeneration capacity of the native heart [1–3]. In an attempt to improve MI treatment, cardiac tissue engineering that combines biomaterial scaffolds, cells and bioactive molecules with the aim of regenerating artificial cardiac tissue constructs has emerged as a promising approach [4]. The cardiac scaffolds play an important role in providing structural support for cell adhesion, pathways for cell communication and convenience for nutrition/waste penetration [5].

To ensure these functional properties, the scaffold materials should not only mimic the elasticity of native myocardium but also have controlled degradation rates to favor tissue regeneration [6]. In the past few years, various polymers have been investigated for cardiac tissue engineering, including synthetic polymers (e.g., polycaprolactone (PCL), polylactic acid (PLA), polyglycolic acid (PGA), poly(lactic-co-glycolic acid) (PLGA), polyurethanes (PU)) [7–9] and natural polymers (e.g., collagen, gelatin, fibrinogen, alginate, chitosan, and silk) [10–12]. However, the majority of these traditional synthetic polymers possess high stiffness (modulus in the MPa–GPa range) and incompatible degradation properties (bulk degradation resulted in unexpected collapse) [13]. In spite of showing good biocompatibility and

* Corresponding author.
** Corresponding author. Key Laboratory for Biomechanics and Mechanobiology of Ministry of Education, Beijing Advanced Innovation Centre for Biomedical Engineering, School of Biological Science and Medical Engineering, Beihang University, Beijing 100083, China.
E-mail addresses: lizhenwang@buaa.edu.cn (L. Wang), yubofan@buaa.edu.cn (Y. Fan).

non-immunogenicity, natural polymers generally lack stability and sufficient mechanical strength to withstand loading conditions during cardiac cycles [14]. To address these challenges, poly(glycerol sebacate) (PGS) is an attractive excellent candidate to serve as the cardiac scaffold material due to its biocompatibility, tunable mechanical properties and biodegradation properties [15–17]. Additionally, the elastic modulus of PGS is between 0.025 and 1.2 MPa depending on the curing conditions, which is matched to that of the human myocardium (0.02–0.5 MPa) [18, 19].

Although exhibiting many advantages, like most degradable polymers, PGS is lack of electroactivity which is essential to promote the recovery of excitation-contraction coupling in the myocardial infarction area. Recent advances in electroconductive materials have paved the way to create conductive scaffolds that could facilitate cell communication, adhesion and proliferation [20]. These conductive materials mainly include carbon nanomaterials (e.g., graphene-based family, carbon nanotubes (CNTs) and carbon dots), electroconductive polymers (e.g., polypyrrole (PPy), poly(3,4- ethylene dioxythiophene) polystyrene sulfonate (PEDOT:PSS) and polyaniline (PANI)), metallic particles (e.g., gold nanoparticles) and silicon nanowires [21–23]. Nevertheless, it is reported that some conducting polymers are brittle, toxic and non-degradable, which restricted their extensive use [24–26]. Among various conductive materials, PANI is one of the appealing choice owing to its facile synthesis, adjustable electrical properties, environmental stability and low produce costs [27]. More importantly, it has been confirmed that PANI showed biocompatibility both in vivo and in vitro, making it suitable by blending with other biodegradable polymers to form conductive scaffolds for myocardial regeneration [28]. For instance, in a recent study, gelatin-PANI nanofibrous composite was prepared by Ostrovidov et al. and they found that the incorporation of PANI enhanced the amplitude of calcium transients and myotube formation [29]. Similarly, a new PU/PANI/SiO$_2$ fibrous patch with shape memory was engineered and it has been demonstrated that the synergism between PANI and SiO$_2$ improved the propagation of electrical signals and self-adhesion on the surface of heart [30].

In addition to select the appropriate materials, structure of the scaffolds is also important when fabricating a cardiac patch, since the native myocardium is mainly composed of parallelly aligned cardiomyocytes (CMs) and cardiac extra-cellular matrix (ECM) whose principal components are type I collagen (89%) and type III collagen (11%) myofibrils of ~100 nm diameters [31]. Such an anisotropic tissue structure is recognized as a key to allow the heart function as a pump with efficient cardiac output [32]. The past few decades have witnessed continuous development of techniques that are driven by the aspiration to prepare various polymer structures containing nanofibers for mimicking the ECM of myocardium. Among these methods, electrospinning has been considered as a versatile and simple approach to fabricate desired nanofibrous scaffolds, because many parameters, such as solution parameters (e.g., solvent types, viscosity, concentration), process parameters (e.g., voltage, flow rate, tip to collector distance), and environmental parameters (e.g., temperature and humidity) could be manipulated and adjusted [33–35].

Unfortunately, PGS was difficult to be prepared into nanofibrous structures, which is another great barrier for its practical applications. The reasons for this fact could be attributed to the insolubility of cured PGS and the glass transition temperature (T_g) of PGS prepolymer is lower than ambient temperature [36]. In order to overcome these obstacles, many polymers like PCL, PLLA, gelatin, thermoplastic polyurethane (TPU) and polyvinylpyrrolidone (PVP) were chosen as carrier polymers and blended with PGS prepolymer to assist the fiber formation [37–39]. But there is a main drawback that the properties of original PGS would significantly change if these blend polymers are not eliminated or the crosslinking step for PGS prepolymer is missed [36]. To meet the requirements of PGS scaffolds with unaltered properties, poly (vinyl alcohol) (PVA), a nontoxic, water-soluble and thermostable polymer, was recently introduced as a carrier, which endowed

possibility upon electrospinning PGS and could be easily removed by immersion in water [36,40,41].

Here, we firstly present novel random and aligned composite fibrous scaffolds which were fabricated by incorporating different amounts of PANI in PGS/PVA fibers through the blending electrospinning method for cardiac tissue engineering. The surface topography, physicochemical properties, mechanical performance, degradation properties and conductivity of the PGS/PANI fibrous sheets were characterized in detail. And H9c2 rat cardiomyocytes were seeded on the biomimetic mats with PANI in different concentrations to evaluate the cell cytocompatibility, proliferation and alignment. Finally, the PGS/PANI fibrous films were subcutaneously implanted into Wistar rats to assess their biocompatibility and degradation in vivo. It is hypothesized that the engineered fibrous patch could provide elasticity, electroactivity, biocompatibility and anisotropic mechanical properties similar to natural myocardial tissue.

2. Materials and methods

2.1. Materials

Glycerol (analysis pure) and sebacic acid (analysis pure) were purchased from Sinopharm Chemical Reagent Co., Ltd., China. Lipase from porcine pancreas and Polyaniline (emeraldine salt) composite (20 wt% polyaniline on carbon black) were obtained from Sigma-Aldrich (Shanghai) Trading Co. Ltd. Poly (vinyl alcohol) 1788 was bought Shanghai Aladdin Biochemical Technology Co., Ltd. 1,1,1,3,3,3-Hexafluoro-2-propanol (HFIP) 99.5% and anhydrous ethanol (analysis pure) were acquired from Macklin Biochemical Co., Ltd., China. Glutaraldehyde and Phosphate Buffer Saline (PBS) powder was gained from Beijing Solarbio Science & Technology Co., Ltd., China.

2.2. Synthesis of PGS prepolymer

Equimolar glycerol and sebacic acid were weighed and added into a three necked flask and reacted for 24 h under nitrogen atmosphere at 130 °C. Then a vacuum pump was connected to the flask and vacuumed once every 0.5 h for another 24 h. Finally, PGS prepolymer was synthesized and poured into beakers for next use.

2.3. Fabrication of random and aligned fibrous PGS/PANI scaffolds

PGS/PANI nanofibrous scaffolds were fabricated by electrospinning method (Fig. 1). The first step was the preparation of electrospinning solution. PVA powder (0.48 g) was completely dissolved in 4 mL deionized water with stirring for 3 h at room temperature, followed by adding PGS prepolymer (0.48 g) and HFIP (6 mL). The mixture was stirred for another 4 h until completely dissolved. Subsequently, different loadings of PANI (1.2, 1.6, 2, 2.4% (w/v)) were added to the prepared PGS/PVA solution, respectively. The resulting electrospinning solution were mixed overnight and placed in an ultrasonic cleaning machine for 20 min to ensure the PANI particles homogeneously dispersed in the PGS/PVA solution. The second step was the electrospinning. A commercial electrospinning equipment (Yunfan Technology, Tianjin, China) was employed to fabricate fibrous sheets containing random or aligned fibers. The solution was sucked into a 10 mL syringe with a 21G blunt stainless-steel needle. Then the mixture was pumped at a flow rate of 1.2 mL/h and PGS/PVA/PANI fibers were formed under applied voltage, which was fixed to +15 kV/−4 kV. Random fibers were deposited on a metal plate wrapped with aluminum foil and aligned fibers were collected on a high-speed rotating mandrel (2000 rpm) wrapped with aluminum foil. The distance between the needle and a collector was maintained constant at 18.5 cm. Temperature and relative humidity were controlled at 32 °C and 25% using a dehumidifier. After HFIP and water were evaporated for several days, the fibrous sheets with different PANI contents were taken off from the aluminum foil.
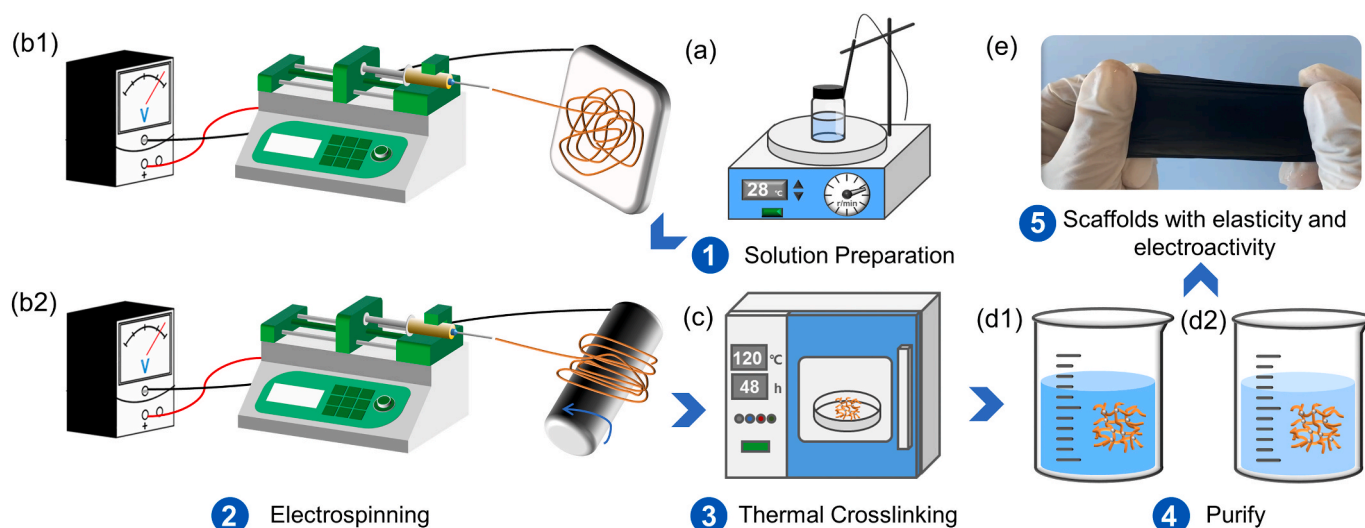
Fig. 1. Fabrication of fibrous PGS/PANI scaffolds. (a) Electrospinning solution was prepared by dissolution and agitation. (b1) The Random fibrous scaffolds were electrospun and collected on a stationary plate. (b2) The Aligned fibrous scaffolds were electrospun and collected on a rotating cylinder with high speed. (c) The fibrous sheets were thermal crosslinked at 120 °C for 48 h. (d1) Samples were purified by water for 12 h. (d2) Samples were washed by anhydrous ethanol for 5 min. (e) Random and aligned biomimetic fibrous scaffolds with elasticity and electroactivity were obtained.

The third step was the thermal crosslinking. Fibrous mats were transferred to a vacuum drying oven and cured at 120 °C under vacuum of −3 MPa for 48 h. The fourth step was the water wash and ethanol wash. The crosslinked scaffolds were soaked in deionized water with gentle agitation at room temperature for total 12 h to remove soluble PVA. The water was changed twice after immersion for initial 3 h and 6 h. Then the water washed scaffolds were dipped in anhydrous ethanol with gentle stir for 5 min to eliminate unreacted PGS prepolymer. Finally, the random and aligned fibrous PGS/PANI scaffolds were acquired after drying the washed scaffolds in drying oven.

2.4. Characterization of fibrous PGS/PANI scaffolds

The morphology of the fibrous PGS/PANI scaffolds were observed by scanning electron microscope (SEM), and their chemical structures, thermal properties, wettability, hemocompatibility and degradation behavior were characterized by Fourier transform infrared spectroscopy (FTIR), differential scanning calorimetry (DSC) and water contact angle measuring device, hemolytic activity test and degradation test, respectively. The detailed processes were showed in the Supplementary Information.

2.5. Electrical conductivity analysis

Cyclic voltammetry (CV) of PGS/PANI scaffolds was conducted on an Electrochemical Workstation (PGSTAT302 N, Metrohm Autolab, Switzerland) employing a three-electrode system. Samples were cut into a 1 cm^2 square sheets and clamped with a platinum plate electrode, which served as a working electrode. Moreover, the counter electrode was a platinum plate, and the reference electrode was saturated calomel electrode. Electrochemical measurements were performed with a scan rate of 10 mV/s using $K_3[Fe(CN)_6]$ electrolyte solution. Different scan rates were also applied on 2.4% (w/v) PGS/PANI scaffolds to examine conductivity. In addition, the electrical conductivity of the spinning liquids with different PANI contents was measured by a conductivity analyzer (DDS-307A, LEICI, China).

2.6. Mechanical testing

Tensile testing of PGS/PANI fibrous scaffolds with different PANI ratios was performed on a mechanical testing system (PBF-300S, CARE Measurement & control) equipped with 300 N sensors. To simulate environment in vivo, mechanical properties of the scaffolds were accomplished in both dry (at room temperature) and wet (after being immersed into 37 °C water) conditions. The fiber mats were cut into dog bone shaped test specimens using a laser cutting machine with outer dimensions (35 mm(l) × 6 mm(w)) and a narrow region (12 mm(l) × 1.5 mm(w)). The thicknesses of the samples were approximately 0.2 mm and measured using a thickness gauge. At least 3 specimens for each group were tested for each group at a speed of 5 mm/min until failure. For anisotropic scaffolds, the samples were measured in two directions; one parallel to the fiber's direction as the preferred direction (PD) and the other perpendicular to the fiber alignment as the cross-preferred direction (XD). The anisotropy of scaffolds was defined as the value in the PD direction by the XD direction. The ultimate tensile strength (UTS), elastic modulus and failure strain were obtained from the plotted stress−strain curves. Besides, the morphology of random and aligned fibrous scaffolds at break was evaluated using SEM. For cyclic tensile test, the mats were stretched to 8% initial strain at a constant velocity of 5 mm/min for 10–50 cycles at room temperature to check reversibility of the scaffolds. All samples were cut into dog bone strips and their dimensions were in accordance with those in the previous uniaxial tensile test.

2.7. In vitro degradation test

The in vitro degradation studies of PGS/PANI fibrous sheets were undertaken for 1, 2, 6, 10 and 16 days. In brief, all samples were cut into disks (n = 3, 8 mm in diameter, about 0.3 mm in thickness) and weighed as W_0. Then they were soaked in 5 mL PBS solution with 2000 U/mL lipase and shaken at 100 rpm in a shaker at 37 °C. After predetermined time intervals, the samples were taken out, rinsed with deionized water and dried. Their weights were measured as W_1. The percentage of mass loss was calculated by Weight loss (%) = $(1 - W_1/W_0) \times 100\%$. It was notable that the mass loss rate was the average of three similar samples with same PANI content. In addition, the morphologies and microstructures of the degraded scaffolds were investigated by SEM.

2.8. H9c2 cell viability, adhesion and proliferation on nanofibrous sheets

H9c2 cells were cultured and the detailed methods were displayed in the Supplementary Information. PGS/PANI scaffolds with 10 mm

diameter and 200 μm thickness were employed for cell seeding. All fibrous sheets were sterilized by 70% ethanol wash and UV exposure for 30 min on each side. Before cell seeding, the scaffolds were dipped in complete culture medium for 1 h H9c2 cells were seeded on mats at a density of 1×10^4 cells/cm^2 in 24-well plate. The medium was changed every other day. The cell viability of H9c2 cells was assessed by a live/dead viability kit (Biorigin (Beijing) Inc.) according to the manufacturer's instructions after 24 h culture. Working solution was prepared beforehand by mixing 30 μL calcein AM, 5 μL propidium and 10 mL PBS together using vortex mixer. And then the scaffolds with different composition were washed by DPBS twice and incubated in the working solution for 20 min at 37 °C. Fluorescent images were captured by an inverted fluorescence microscope (IX70, Olympus) and followed cell viability was determined by analyzing the number of dead and live cells with ImageJ software (NIH).

The proliferation rate of H9c2 cells on PGS/PANI fibrous scaffolds was investigated by a Cell counting kit-8 reagent (CCK-8, Dojindo, Kumamoto, Japan) on the basis of the manufacturer's guidelines after incubating 24, 48 and 72 h. In brief, each scaffold was seeded with 1×10^4 cells suspended in complete medium. The culture medium was substituted with 10% (v/v) CCK-8 reagent at each corresponding time point after culturing 1, 2, and 3 days. 100 μL solution from each well was transferred to a 96-well plate after incubating for 3 h at 37 °C in CO$_2$ cell incubator. Finally, the absorbance of each sample at a wavelength of 540 nm was read by a multifunctional microplate reader (Varioskan LUX, Thermo Fisher Scientific, USA).

To evaluate the adhesion of H9c2 cells cultured on various PGS/PANI fibers, PGS/PANI scaffolds which had seeded H9c2 cells for 72 h were taken out from the incubator and washed with PBS. Subsequently, the samples were fixed with 2.5% glutaraldehyde for 1 h at ambient temperature. Then these samples were washed with PBS again and dehydrated using the gradient of concentration of ethanol from 50% to 100%. Finally, the samples were attached to conductive tapes, coated with a thin layer of gold and viewed with SEM (QuantaTM, FEG) at an operating voltage of 10 kV.

2.9. In vivo biodegradation and biocompatibility of PGS/PANI fibrous sheets

All animal experiments were implemented in compliance with the guidelines for the care and use of research animals formulated by the Beihang University Animal Experiment Ethics Review Committee. Eighteen female Wistar rats weighing about 200 g were purchased from SPF (Beijing) Biotechnology Co., Ltd. Ten of them were used for in vivo biocompatibility evaluation and the remaining rats were for in vivo biodegradation assessment of PGS/PANI fibrous scaffolds. Before subcutaneous implantation, the fibrous films were cut into 4 mm wide and 12 mm long strips. Then they were washed by distilled water, dried in 50 °C drying oven to eliminate moisture and sterilized by ultraviolet light on each side for 60 min. After anesthetizing by injection with 3% pentobarbital sodium (1 mL/kg), five 1.2–1.5 cm incisions were made on the two sides of the rat's back. The prepared random and aligned fibrous PGS/PANI films were successively implanted into the subcutaneous pockets of each rat. And the wounds were closed using degradable sutures. Subsequently, water and food were provided for the experimental rats in time to help them recover from the surgery. After implantation for 1, 2, 4 and 8 weeks, the rats were sacrificed and samples with surrounding tissues were harvested. The samples of ten rats were embedded in paraffin, sectioned into 3 μm thick slides and observed by Hematoxylin and Eosin (H&E) staining and Masson's trichrome staining images. For the samples of rest eight rats, the surrounding tissues were peeled off from the scaffolds and these degraded scaffolds were rinsed with deionized water for three time. After lyophilization, the samples were sputtered with gold and their microstructure and morphology were imaged by SEM (QuantaTM, FEG) under high vacuum.

2.10. Statistical analyses

All quantitative data in this study were presented as mean ± standard deviation (Mean ± SD). Analyses were conducted on these data by Origin 2018 (Origin Lab) and IBM SPSS Statistics 25 (International Business Machines Corporation). Student's T-test was carried out to examine the independent samples in two groups. One-way and two-way analysis of variance (ANOVA) was adopted with Least Significant Difference (LSD) to compare groups more than two. It was considered statistically significant differences when *$P < 0.05$.

3. Results and discussion

3.1. Preparation and morphologies of PGS/PANI fibrous scaffolds

For the purpose of mimicking the human myocardium which consists of fibrillary collagen-based ECM and conductive Purkinje fibers, random and aligned nanofibrous scaffolds were fabricated by electrospinning in this study. All fiber sheets showed a smooth and defect-free morphology with the homogenous fiber diameters after carefully tuning the electrospinning parameters. However, it was not easy to optimize the final electrospinning parameters. Based on the previously established protocols, we initially attempted to prepare PGS/PVA fibrous membranes at 1.2 mL/h flow rate under 15 kV with the 16%w/v concentration and used HFIP as the solvent. Beyond our expectations, as shown in Fig. S1a, the SEM image demonstrated flat PGS/PVA fiber belts that were difficult to distinguish and they almost sticked together. It was assumed that the higher concentration, poorer solubility of PVA in HFIP and insufficient applied voltage were the causes of the wide PGS/PVA fibers. In general, thinner fibers will be formed as the applied voltage is increased. By decreasing the polymer concentration, both viscosity and surface tension of the polymer solution will be reduced, also supporting the formation of thinner fibers. The boiling point of HFIP is only 59 °C and it can be easily evaporated [42]. Additionally, water is the most favorable solvent for PVA due to the abundance of free hydroxyl in its structure and hydrogen bonding [43]. Although the volatility of water is low at room temperature and it has high dielectric constant, which limited its use as electrospinning solvent, utilizing higher room temperature is helpful to accelerate the evaporation and improving applied voltage makes it possible for the formation of stable jet, both of them are efficient strategies. Hence, we modulated the applied voltage as 19 kV and lowed the polymer concentration to 12%w/v. A mixture of water and HFIP in the proportion of 1:1 was creatively proposed as the electrospinning solution in order to achieve the optimal formulation for electrospinning PGS/PVA. Since a recent study that was carried out by Saudi et al. has suggested that PVA/PGS scaffolds with 50:50 ratio exhibited better cell adhesion and proliferation when compared with 60:40 samples [44], we keep 50:50 PGS/PVA ratios the same in the throughout the research.

Different from electrospun fibers with 16%w/v polymer concentration, the 12%w/v electrospun scaffolds had an average diameter of 3391 ± 100 nm showing flat ribbon structure in Fig. S1b. According to our prior experience, fast evaporation of the solvent could lead to the fibers collapse, and thus formed flattened fibers. This also could be verified by the previous reports [45,46]. The influence of the solvent system on fiber diameters was also measured from different SEM images (Fig. S1c and d) with the help of Image J. It was observed that the 12%w/v PGS/PVA fibers using a mixed solvent system consisting of water and HFIP had an average diameter of 468.16 ± 166.98 nm, and for 16%w/v PGS/PVA scaffolds, an increase in the fiber average diameter up to 1699 ± 24 nm was observed. Therefore, these results confirmed our hypothesis after better control of electrospinning process. Upon the data analysis of above pre-experiment basis, the formal electrospinning parameters were set as 19 kV applied voltage, 1.2 mL/h flow rate, 15 cm distance between the spinneret and the collector, 32 °C ambient temperature, 12%w/v PGS/PVA concentration and mixed solvent including

HFIP and water.

Fig. 2a displays representative macrography of PGS/PVA/PANI scaffolds containing different concentrations of PANI after electrospinning. The color of the fibrous sheets turned darker as the fabrication process went on and more volume contents of PANI added into the PGS/PVA solutions. The effect of the different amount of PANI on the morphology behind electrospinning and ethanol wash was investigated by SEM, and their micrographs were shown in Fig. 1b, along with their fiber diameter distributions were shown in Fig. 2c. Based on the results, bead-free and smooth fibers with highly uniform diameters were successfully fabricated for all electrospun fibrous scaffolds. PANI particles with irregular shape are homogeneously dispersed within the PGS/PVA fibers due to the hydrogen bond interactions between these polymers. The mean diameters of random PGS/PVA scaffolds with 0% (w/v) PANI, 1.2% (w/v) PANI, 1.6% (w/v) PANI, 2% (w/v) PANI and 2.4% (w/v) PANI estimated 468.16 ± 166.98, 461.39 ± 126.76, 469.79 ± 123.57, 472.36 ± 134.63, and 426.80 ± 140.17 nm, respectively. Generally, within an appropriate range, lower PANI concentration favors the production of thinner fibers. But for 2.4% (w/v) PANI fibers, the diameters obviously decreased, which could be attributed to that conductive PANI particles enhanced the stretching of PGS/PVA fibers. If the content of PANI exceeded 2.4% (w/v), the fibers would be difficult to form. Because PANI molecules have rigid backbones, an excessive PANI contents could result in poor solubility and blocking of the nozzle. Aligned fibrous PGS/PVA/PANI scaffolds without bead defects were obtained by collecting on a rapidly rotating mandrel. The diameters of aligned 1.2%, 1.6%, 2% and 2.4% (w/v) PANI fibers were about 521.42 ± 139.48,

474.46 ± 132.05, 564.88 ± 158.20 and 465.22 ± 127.90 nm, while the diameters of PGS/PVA fibers were 206.51 ± 53.5 μm. These results indicated that the addition of PANI increased electrospinning concentration, which made fibers thicker, and more PANI meant higher conductivity. Some publications also revealed that higher conductivity resulted in decreasing fiber diameters. For example, Abedi et al. fabricated chitosan (CS)/PVA scaffolds loaded with multi-wall carbon nanotubes (MWCNTs) for cardiac tissue engineering [47]. They reported that five times increase in the conductivity of 2 wt% MWCNT to PVA/CS solutions could result in 3 times decrease in the fiber diameters compared to the CS/PVA scaffolds [47]. Thus, it was the intricate interplay of concentration and conductivity that affected the diameter and morphology of PGS/PVA fibers when incorporating PANI particles. In addition, it was found that the diameters of aligned PGS/PVA fibers were significantly lower than that of randomly oriented fibers. The major reason of this phenomenon may be that the rotating drum with high speeds developed a centrifugal force in the region near the mandrel, which elongated the fibers and made them narrow before deposited on the drum. According to previous works, there are significant differences of fiber diameters among the various carrier polymers for PGS fibrous scaffolds such as PGS/PU (1389 ± 332 nm) [48], PGS/PVP (0.85 ± 0.58 μm) [49], PGS/PLLA (332 ± 103 nm) [50] and PGS/PCL (2.3 ± 0.3 μm) [51]. The sub-micron fiber diameters of our PGS/PVA/PANI scaffolds were in congruence with that of collagens and elastin nanofibers which assembled into cardiac ECM.

After electrospinning, the most important step was the crosslinking, because crosslinking not only ensured enough elastic elasticity of PGS
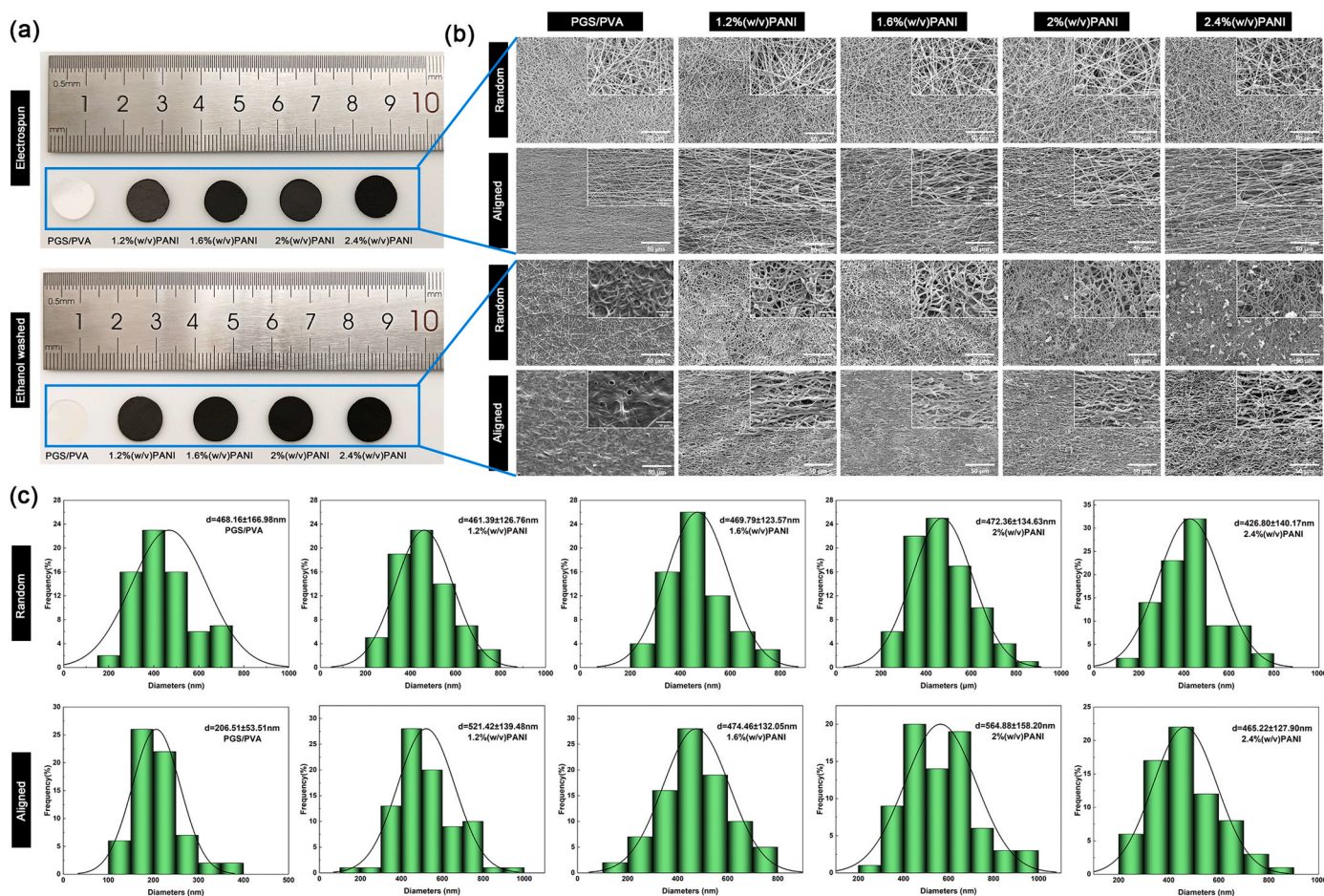

Fig. 2. Topographical evaluation of random and aligned PGS/PVA/PANI scaffolds. (a) Optical images of representative electrospun PGS/PVA/PANI samples and ethanol washed PGS/PANI containing different concentrations of PANI. (b) SEM images of random and aligned PGS/PVA/PANI and PGS/PANI fibrous sheets after electrospinning and ethanol wash. (c) Fiber size distributions of random and aligned electrospun PGS/PVA/PANI scaffolds with different PANI content.

for cardiac tissue engineering scaffolds, but also eliminated the cytotoxic effect of PGS prepolymer without treatment [36]. Subsequently, water and ethanol purification were continued to accomplish for preparing PGS/PANI scaffolds, and the final morphologies and fiber diameters of the fibrous scaffolds after these stages were analyzed based on the SEM images and shown in Fig. 2b and c. Both random and aligned ethanol washed scaffolds showed typical circular shape. It was a direct challenge to holding the fibrous structure with defined edges during thermal crosslinking because high temperatures could lead PGS prepolymer easily to soften and fuse. However, the melting phenomenon in the prepared scaffolds disappeared by adding PANI. As shown in Fig. 2b, PGS/PVA fibers lost its fibrous structure along with the reduction in void spaces upon crosslinking at 120 °C for 48 h. As shown in Fig. S2, the Gaussian distribution histogram revealed that the fiber diameters of the final random 1.2%, 1.6%, 2% and 2.4% (w/v) PANI scaffolds were 888.96 ± 290.85, 829.80 ± 275.24, 579.56 ± 178.76 and 500.94 ± 149.36 nm. And the final aligned 1.2%, 1.6%, 2% and 2.4% (w/v) PANI scaffolds had an average diameter in the range of 905.26 ± 288.82, 870.19 ± 238.68, 645.14 ± 183.60 and 749.86 ± 183.60 nm. In

comparison with the diameters of electrospun fibers, both diameters of crosslinked random and aligned scaffolds obviously elevated due to the fiber fusion. The finding was a clear manifestation of the essential component of PNAI in the maintaining of the defined fiber structure. Furthermore, as show in Fig. S3, taking 2.4% (w/v) PANI scaffolds as example, water washing and ethanol appeared to have little effect on fiber morphology and microstructure of the crosslinked scaffolds compared to the significant changes observed after crosslinking.

3.2. FTIR characterizations

The chemical structure of the pure PGS prepolymer, PVA, PANI, as well as non-crosslinked PGS/PVA fibers and typical PGS/PVA/PANI scaffolds were evaluated using FTIR analysis in Fig. 3a. The FTIR spectra of the synthesized PGS prepolymer in this study were in accordance with those in previous literature [15,52]. The main peaks were located at 1737 cm^{-1} corresponding to C]O stretching vibration and 1172 cm^{-1} related to C-O stretching, which indicating the formation of the ester bond. As can be seen, for pure PVA, the stretching vibration of the C-O
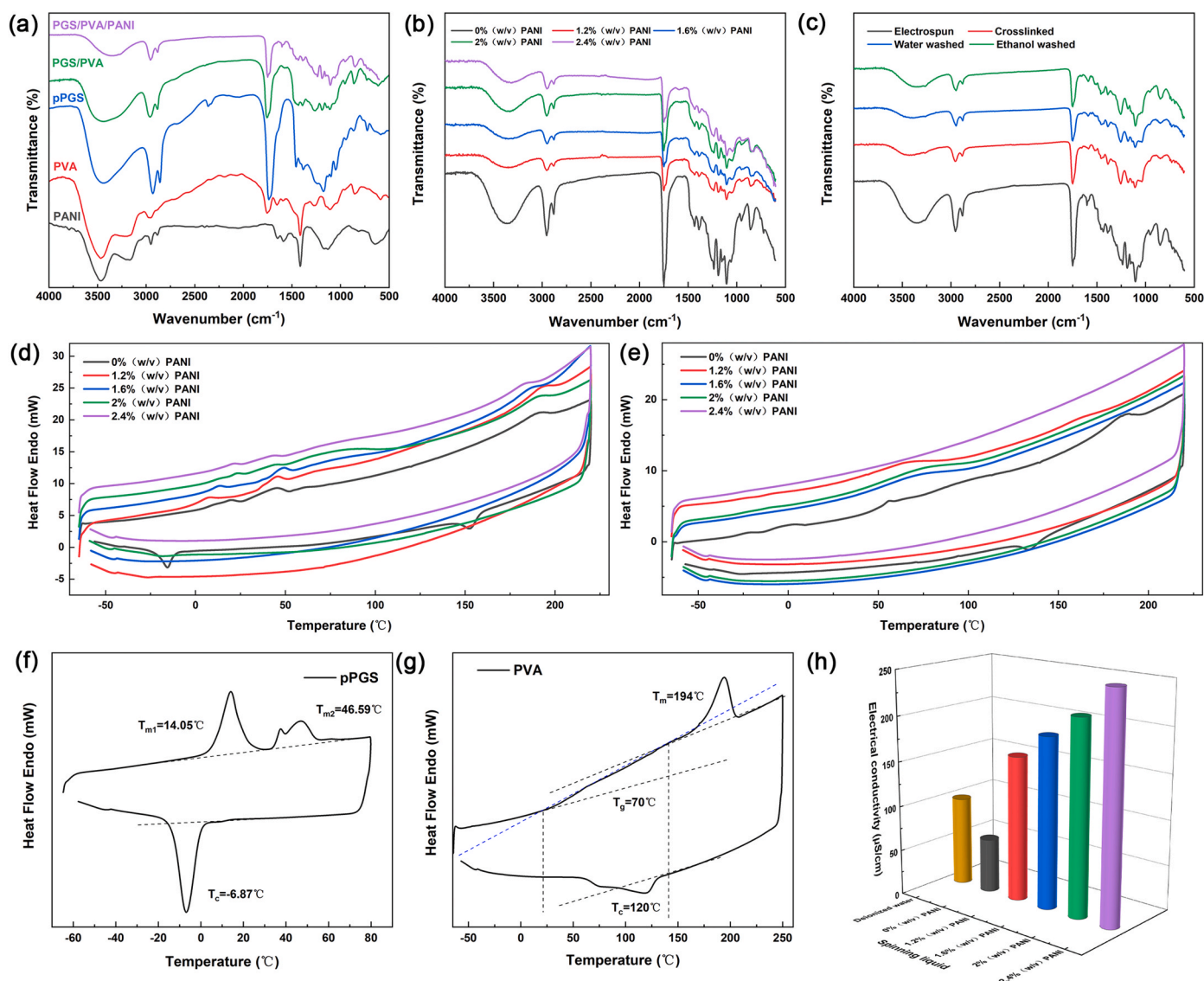

Fig. 3. Characterization of PGS/PVA/PANI scaffolds. (a) FTIR spectra of the PGS prepolymer, PVA, PANI, electrospun PGS/PVA and PGS/PVA/PANI scaffolds. (b) FTIR spectra of electrospun PGS/PVA/PANI samples with different PANI content. (c) FTIR spectra of PGS/PANI samples after different fabrication steps. (d) DSC curves of the electrospun PGS/PVA/PANI fibrous samples. (e) DSC curves of the PGS/PANI fibrous samples after ethanol wash. (f) DSC curves of PGS prepolymer. (g) DSC curves of pure PVA. (h) The histogram of the electrical conductivity for electrospinning solution with different PANI concentrations.

appeared at 1108 cm^{-1}, the infrared bands at 1415 cm^{-1} and 850 cm^{-1} were associated with CH$_2$ bending and stretching, respectively. Another peak detected at 1753 cm^{-1} might be correlated with the residual vinyl alcohol monomers from the hydrolysis of poly(vinyl acetate) (PVAc) [47]. Additionally, a broad peak was observed from 3000 cm^{-1} to 3600 cm^{-1} in the FTIR spectrum of both PVA and PGS prepolymer due to the stretching of abundant O-H groups. Electrospun PGS/PVA fibrous scaffolds demonstrated all critical bands of PGS prepolymer and PVA, like the asymmetric and symmetric shoulder stretching vibration peaks of –CH$_2$ at 2958 cm^{-1}, and 2883 cm^{-1} for PGS and wide hydroxyl absorption peak for PVA. It could be found from the FTIR results that the PGS/PVA fibers and PGS prepolymer had very similar spectra since the chemical configurations of PVA resembled PGS prepolymer. Pure PANI samples were also solely tested to assess their chemical functional groups. The representative infrared bands of PANI included: 1644 cm^{-1} (C]C quinoid stretching), 1585 cm^{-1} (C–N quinoid stretching), 1482 cm^{-1} (C]C benzenoid rings stretching vibration), 1417 cm^{-1} (C–C quinoid ring vibration) and 3480 cm^{-1} which might be ascribed to the groups of the doped acid [53,54].

Fig. 3b shows the FTIR spectra of the electrospun PGS/PVA/PANI scaffolds with various ratios of PANI including 0, 1.2, 1.6, 2, and 2.4% (w/v). In consideration of the low content of PANI in fibrous scaffolds, strong peaks of PGS and PVA overlapped some peaks associated with PANI, thus these FTIR curves were almost similar. But with the incorporation of PANI in PGS/PVA fibers, the intensity of the peak at 3350 cm^{-1} which was respective to the O-H stretching decreased, because the intermolecular distances might increase and hydrogen bonding interaction weakened. In order to assess the effect of the fabrication process on the chemical functional groups of PGS/PANI scaffolds, the PGS/PANI samples fabricated by different steps including electrospinning, crosslinking, water wash or ethanol wash were measured using FTIR method (Fig. 3c). Similar characteristic peaks could be observed in these FTIR spectra. However, comparing to the spectra of crosslinked PGS/PVA/PANI scaffolds, the broadband of the hydroxyl group (–OH) and strong C]O peaks in the electrospun scaffolds significantly shrunk. The findings suggested that some PGS molecules had crosslinked with each other and a portion of PVA and PGS molecules might bound together through the hydrogen bonds.

3.3. Thermal properties

Since the thermal properties of the polymers were important to explain the PVA content in the composite scaffolds, the thermal behaviors of the synthesized PGS prepolymer and PVA were first studied employing the DSC. As seen in Fig. 3f, the synthesized PGS prepolymer showed two melting temperatures, T_{m1} at 14.05 °C and T_{m2} at 46.59 °C, and a T_c at −6.87 °C. It was speculated that the two melting temperatures might be correlated with the sebacic acid and glycerol fragment, respectively. As revealed by some previous literature, T_m and T_c of PGS could be changed according to the variations of the curing conditions [55,56]. As shown in Fig. 3g, PVA used in the blended scaffolds indicated a T_g of around 70 °C, a broad endothermic peak at about 194 °C corresponding to its melting temperature and T_c around 120 °C. These characteristic temperatures of PVA were profoundly affected by the crystallinity and degrees of hydrolysis of the PVA [43,57,58].

The effect of PANI particles with various concentrations on the thermal transitions of the electrospun PGS/PVA fibrous sheets was presented in Fig. 3d obtained from DSC analysis. The thermogram of electrospun PGS/PVA scaffolds displayed three distinct endothermic peaks at 20 °C, 45 °C and 190 °C, respectively, which could be associated with the melting points of the PGS prepolymer and PVA. The thermogram confirmed that the composite scaffolds are constituted by two components, PGS prepolymer and PVA. From the DSC curves of the PGS/PVA/PANI fibers, it could be seen that doping the PGS/PVA fibers with different content of PANI resulted in a small but obvious shift in T_{m1}, T_{m2} and T_{m3}. For example, T_{m1} shifted from about 8 °C (1.2% (w/v)

PANI) to 21 °C (2.4% (w/v) PANI) and T_{m3} changed from about 194 °C (1.2% (w/v) PANI) to 183 °C (2.4% (w/v) PANI). Additionally, both the endothermic enthalpy and exothermic enthalpy of the composite scaffolds became weakened and even difficult to be observable with the increase of the PANI concentrations. DSC measurements were also performed to determine the T_m, T_g and T_c of the final PGS/PANI scaffolds with different contents of PANI after electrospinning, thermal crosslinking, water and ethanol purification. The DSC thermograms were exhibited in Fig. 3e. The PGS/PVA scaffolds indicated two glass transitions, The first transition observed between −29 and −20 °C corresponded to the glass transition of PGS, while those between 70 and 90 °C corresponded to the glass transition of PVA. And other endothermic peaks of the final PGS/PVA scaffolds appeared at 1 and 186 °C, with an exothermic peak at 135 °C. It was identified that the original crystallization peak for PGS prepolymer disappeared due to the crosslinking steps. Besides, with increasing the PANI content in the PGS/PVA fibers after purification, both the melting peaks and crystallization peaks of the PGS/PVA/PANI scaffolds were difficult to distinguish and nearly vanished, especially for the PGS/PVA/PANI scaffolds with high PANI content such as the 2.4% (w/v) PANI. These DSC results suggested that the washing procedures are effective for removing PVA from the PGS/PVA/PANI scaffolds but there were some PVA still existed in the PGS/PVA scaffolds. The reasons might be that the PGS/PANI scaffolds have clear fibrous structures which were convenient for the permeation of water, while PGS/PVA scaffolds were difficult to maintain their fibrous structure and tended to form flat surfaces during crosslinking which made PVA trapped in the matrix. Although some PVA may be incorporated into the final fibrous scaffolds, it had low impact on the cytocompatibility or mechanical properties of the scaffolds [36].

3.4. Hydrophilicity

The hydrophilicity or hydrophobicity of the scaffolds is one of the most important factors in affecting the cell adhesion, migration and growth in tissue engineering since the hydrophilicity plays a vital role in regulating the proteins adsorption on the scaffolds [59]. The hydrophilicity of the final random fibrous PGS/PANI scaffolds after purification was assessed by measuring the surface contact angle. The results are presented through Fig. 4d and e, where the water contact angles of random PGS/PVA, 1.2% (w/v), 1.6% (w/v), 2% (w/v) and 2.4% (w/v) PANI scaffolds were 85.7 ± 3.2°, 78.5 ± 3.4°, 109.7 ± 8.4°, 129.7 ± 2.8° and 127.3 ± 5.8°, respectively. Thus, by adding PANI into the scaffolds, the water contact angle significantly increased which correlated well with a few literature [28,54,60]. It was because that undissolved PANI particles scattered all over the fibrous scaffolds were able to overshadow the hydrophilic interaction created by the hydroxyl groups [28]. Moreover, the reason why the water contact angle of PGS/PVA was higher than 0% (w/v) PANI might be that the water droplets were easier to penetrate the fibrous 0% (w/v) PANI scaffolds than the intact PGS/PVA scaffolds with fibers fusion. The results for the water contact angle values of the PGS/PANI scaffolds with 1.2% (w/v) PANI content after different steps were presented in Fig. S4. The water contact angle of the scaffolds after electrospinning, thermal crosslinking, water wash and ethanol wash represented 0°, 57.8 ± 14°, 79.5 ± 6.8° and 104.3 ± 10°, respectively. There were significant differences between these fabrication steps. The water droplets penetrated into the electrospun PGS/PVA/PANI scaffolds very easily and quickly due to the high water-soluble ability of PVA, hydrophilic nature of PGS prepolymer and porous structure formed by the connecting fibers. After that, the crosslinking step was necessary to make PGS prepolymer turn into PGS, which not only ensured the elasticity of the composite scaffolds but also avoided the cytotoxic effect of the PGS prepolymer to cells. The following water wash and ethanol wash removed a majority of PVA and residual PGS prepolymer. Consequently, the surface wettability of the PGS/PANI scaffolds obviously decreased.
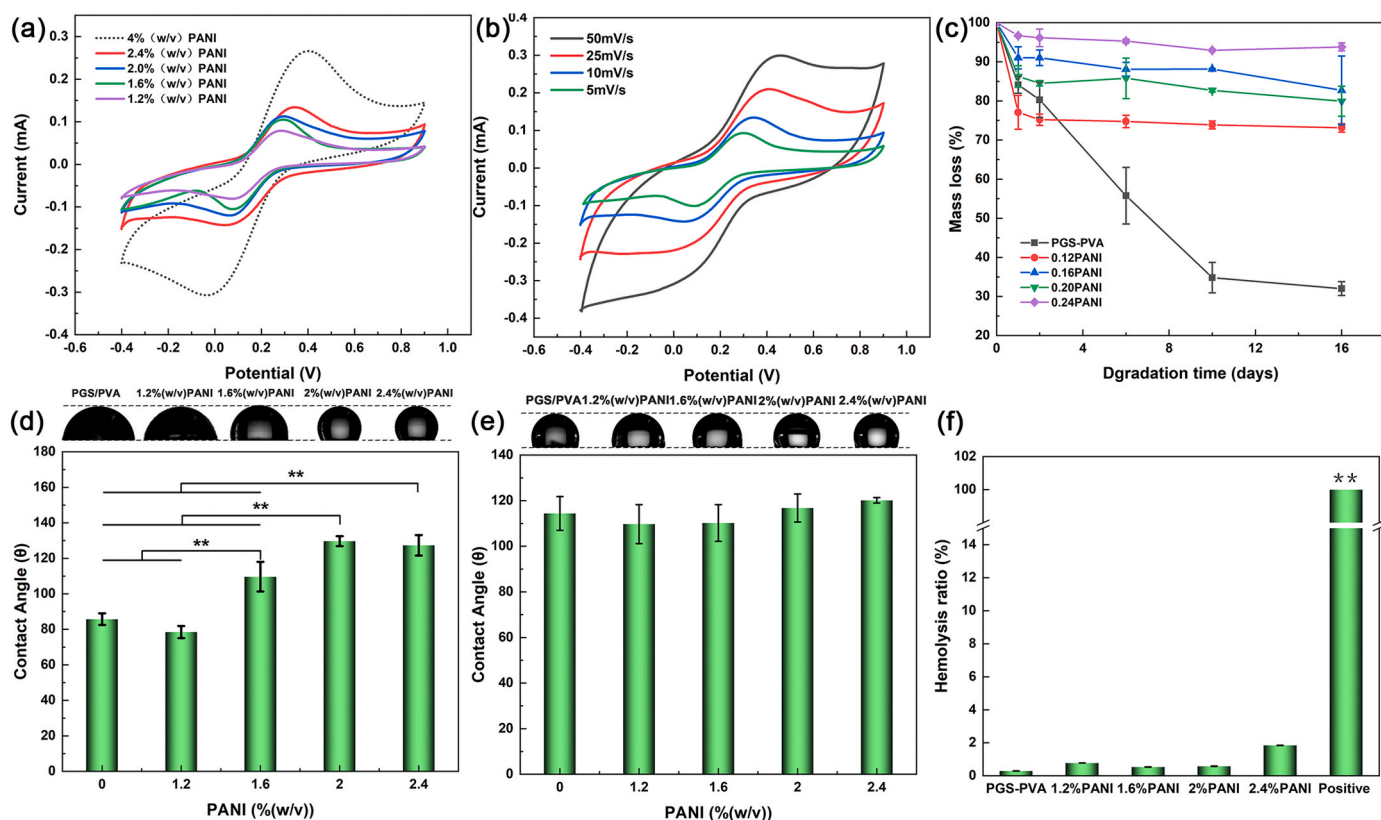
Fig. 4. (a) The CV spectrum of PGS/PANI fibrous sheets in $K_3[Fe(CN)_6]$ solution, scan rate 10 mV/s. (b) The CV curves of PGS/PANI fibrous scaffolds at different scanning speeds. (c) Representative mass loss curves of fibrous scaffolds following 16 days of soaking in PBS with 2000 U/mL lipase at 37 °C. (d) The water contact angles of random fibrous PGS/PANI scaffolds. (e) The water contact angles of aligned fibrous PGS/PANI scaffolds. (f) The quantitative hemolysis ratio of fibrous PGS/PANI mats.

3.5. Electrical properties

With the aim of evaluating the impact of PANI on electrical conductivity, homogeneous electrospinning solutions with different contents of PANI were prepared, and their electrical conductivity were measured using a conductivity meter. As shown in Fig. 3h, the conductivity of the PGS/PVA, 1.2% (w/v), 1.6% (w/v), 2% (w/v) and 2.4% (w/v) PANI were 6×10^{-3}, 1.6×10^{-2}, 1.9×10^{-2}, 2.2×10^{-2} and 2.5×10^{-2} S/m. Based on the results, there was a direct relationship between the contents of PANI and the electrical conductivity of their spinning liquids as it is well known that PANI is a promising conducting polymer with tunable electrical conductivity [61]. Feng et al. prepared a PU/PANI/SiO_2 submicron fiber patch notable for conducting weak electrical signals, they observed that the PU/PANI/SiO_2 spinning liquids had electrical conductivity in the range of 9.8×10^{-3} - 1.8×10^{-2} S/m [30]. It could be found that our PGS/PANI scaffolds had wider conductivity range when comparing with PU/PANI/SiO_2 fibrous scaffolds. Moreover, Qazi et al. have confirmed that PGS/PANI films had similar conductivity with that of the native cardiac tissue, which ranged from 1.6×10^{-1} S/m (longitudinally) to 5×10^{-3} S/m (transversally) [28]. Furthermore, piezoelectric and magnetoelectric effect should be taken under consideration when optimizing these electroactive materials in future studies, which could greatly expand their applications such as biosensors, tissue engineering, drug delivery and brain stimulation [62].

The cyclic voltammetry was then used to investigate the electrochemical properties of PGS/PANI scaffolds including different amount of PANI at a scan rate of 10 mV s^{-1} (Fig. 4a). The CV curves of all PGS/PANI composite scaffolds presented a pair of distinct symmetric redox peaks, especially, PGS/PANI scaffolds with the content of 4% (w/v) PANI exhibits the strongest redox peaks, indicating the fast redox reaction of conductive PANI in the composite. The positive peaks of 1.2%

(w/v), 1.6% (w/v), 2% (w/v) and 2.4% (w/v) PANI scaffolds were located at 0.28, 0.29, 0.30 and 0.34 V, and the negative current peaks of these scaffolds were located at 0.08, 0.08, 0.07 and 0.06 V. Interestingly, some of the published CV curves for PANI composites showed two pairs of redox peaks, which corresponded to the transitions of PANI from the leucoemeraldine to the emeraldine oxidation state, and subsequently from the emeraldine to the pernigraniline state [63–65]. The peak difference may be largely due to the discrepancies of the selected PANI. For example, some PANI used for conductive composites was PANI emeraldine base doped with camphorsulfonic acid, or PANI in the emeraldine salt, whereas in this work PANI (emeraldine salt) composite (20 wt% PANI on carbon black) was employed in order to effectively improve the conductivity of the blend fibrous scaffolds. To assess the relationship between the scan rate and the electrochemical performance of PGS/PANI scaffolds, the CV measurements were also performed in $K_3[Fe(CN)_6]$ solution (Fig. 4b), and different scan rates, ranging from 5 to 50 mV s^{-1}, were used. It was observed that both the current and peak potential were impacted by scan rates. The increase in scan rates accompanied by the augment in peak current, which might be ascribed to that the migration and diffusion of the electrolytic ions were affected by the scan rates.

3.6. Hemolytic activity

The hemocompatibility is one of the environment evaluation indicators for successful cardiac tissue engineering scaffolds because these scaffolds are directly contact with the blood environment. The poor hemocompatibility of the implant material will result in blood coagulation and thrombosis. Here, the hemolytic activity of the fibrous PGS/PANI scaffolds with different PANI content was investigated and the results were displayed in Figs. 4f and S5. As shown in Fig. S5, the

supernatant of PGS/PANI fibrous sheets with various PANI contents demonstrated almost transparent color, similar to the supernatant of the negative physiological saline group, while the positive group containing distilled water appeared bright red. The quantitative analysis of the hemolysis ratio also confirmed the results in Fig. 4f. Apart from PGS scaffolds, The PGS/PANI scaffolds with 1.6% (w/v) PANI had the lowest hemolysis ratio, 0.54%. It was understandable for the findings because both PGS and PVA showed good blood compatibility according to the previous hemolysis assays [19,66,67]. And adding PANI into PGS scaffolds blends didn't significantly enhance their hemolysis ratio. Taken together, these results suggested that PGS/PANI was a kind of promising blood compatible material for tissue engineering scaffolds.

3.7. Mechanical properties

Natural cardiac tissue contractility and relaxation during cardiac cycle are dependent on the anisotropic mechanical characteristics of myocardium. Fibrous tissue engineering scaffolds with different properties electrospun in a defined manner, could serve as the replacement of native myocardium if their mechanical characteristics could be

matched. Here, uniaxial tensile testing under dry and wet conditions was performed to investigate the mechanical properties of the random and aligned PGS/PANI fibrous scaffolds with different PANI contents. Based on the stress–strain curves of these composite scaffolds, ultimate tensile strength, elastic modulus and strain-to-failure were calculated, as seen in Fig. 5a–f.

The elastic modulus of the scaffolds enhanced from 3.20 ± 1.85 MPa for PGS scaffolds to 8.57 ± 7.13 MPa for PGS/PANI blend scaffolds with 2.4% (w/v) PANI content under dry condition, and from 0.65 ± 0.11 MPa to 2.18 ± 1.28 MPa when wet condition was investigated. The presence of more PANI content in the polymer solution increased the elastic modulus and decreased strain-to-failure, this was in agreement with some aforementioned reports [68,69]. For example, PANI-gelatin blend fibers were fabricated by Li et al., and they found that the tensile modulus enhanced from 499 ± 207 MPa to 1384 ± 105 MPa with the incorporation of PANI [68]. Another studies with regard to nanofibrous scaffolds composed of PANI and PCL indicated that the Young's modulus of the fibers increased from 7.2 ± 5.0 MPa for PCL fibers to 55.2 ± 3.6 MPa for PCL/PANI fibers. The reasons for our results may be due to the high intrinsic rigidity of PANI, and the proper interaction
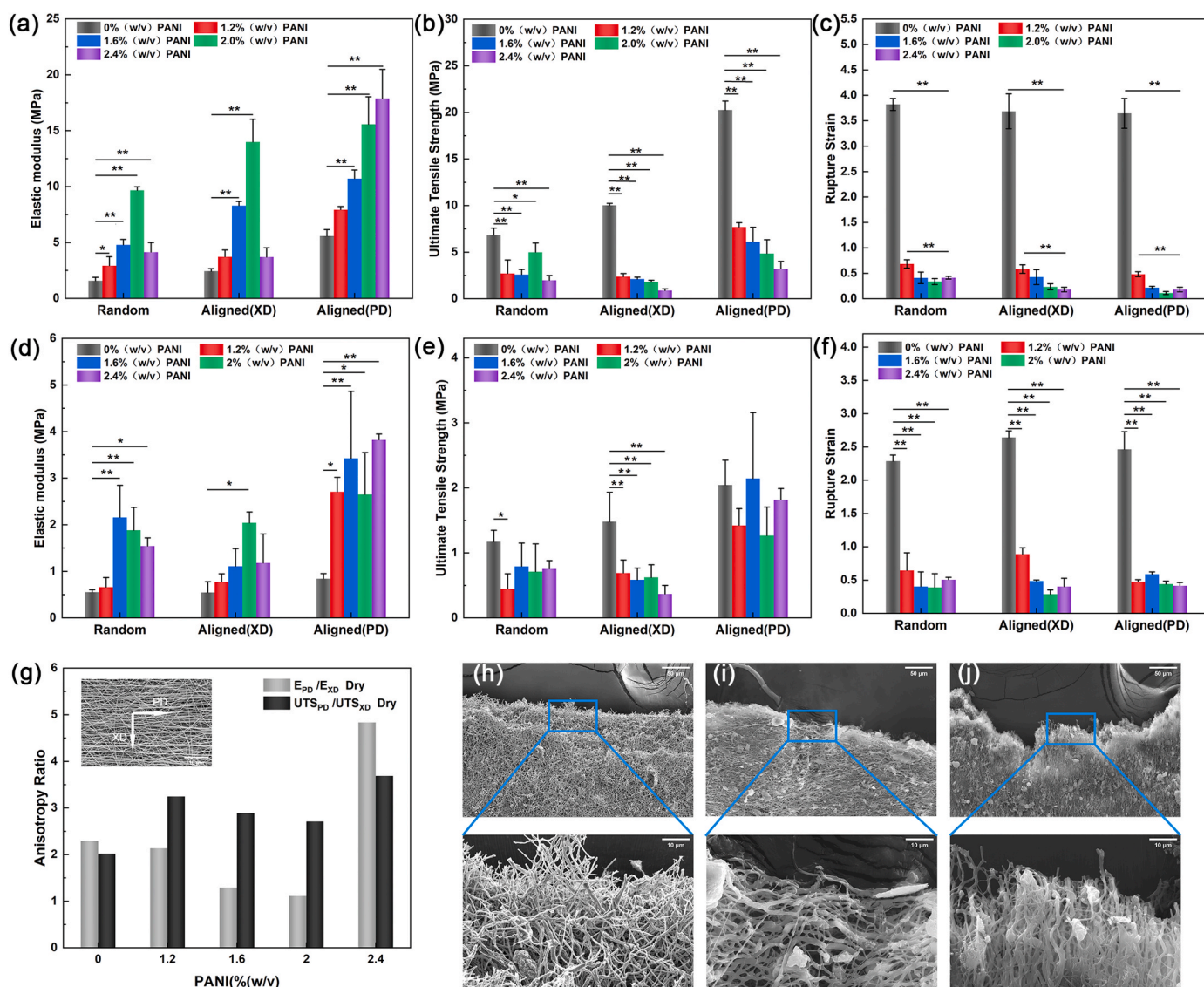

Fig. 5. Uniaxial mechanical testing of random and aligned scaffolds in two directions. (a) Elastic modulus of random and aligned scaffolds in XD and PD direction at room temperature. (b) UTS at room temperature. (c) Rupture strain at room temperature. (d) Elastic modulus of random and aligned scaffolds in PD and XD direction at 37 °C. (e) UTS at 37 °C. (f) Rupture strain at 37 °C. (g) Anisotropy of aligned PGS/PANI scaffolds with varying ratios was measured. (h–j) Fracture morphologies of random and aligned scaffolds in XD and PD direction at room temperature were observed by SEM ($n = 5$, *$P < 0.05$, **$P < 0.001$).

between the PANI particles and the PGS fibers. Additionally, it was noteworthy that 2% (w/v) PANI scaffolds were found to possess the highest elastic modulus in random and XD direction under dry condition. The reasons might be that there was an uneven distribution of PANI particles in different fibrous mats and random fibrous scaffolds had various fiber directions, which may cause correspondingly high standard deviations. Furthermore, it was reported that the Young's modulus of native human myocardium reached several tens of kPa to less than 0.5 MPa [30], so the fabricated PGS/PANI scaffolds possess sufficient stiffness to satisfy the relaxation and contraction strength of natural human myocardium.

However, the tensile strength showed an almost opposite relationship with the addition PANI. The tensile modulus of PGS fibrous mats was 12.36 ± 6.11 MPa and then significantly decreased to 2.03 ± 1.13 MPa for 2.4% (w/v) PGS/PANI scaffolds in dry condition. Similarly, the tensile modulus of PGS scaffolds decreased from 1.57 ± 0.49 MPa to 0.98 ± 0.66 MPa in wet condition. The reasons why PGS scaffolds manifested the maximal tensile modulus were worth exploring. It was speculated that because PGS scaffolds had the highest degree of the fiber fusion among all composite fibrous scaffolds after crosslinking, which approximately formed planar films without interspace between fibers. With increasing the amount of PANI particles, the porosity of the PGS/PANI scaffolds gradually increased and resulted in a decreasing tendency for UTS of the composite scaffolds. Some literature have also reported the addition of doped PANI to polymers impaired tensile strength [29,70]. For example, it was observed by Jeong et al. that a decrease in tensile strength with increasing PANI concentration in Poly(ʟ-lactide--*co*-e-caprolactone) (PLCL) [70]. They thought that doping acid of PANI exerted an important effect on the changes of the mechanical properties of the blend fibrous scaffolds. Overall, nearly all mechanical parameters like elastic modulus and UTS of the PGS/PANI reduced under wet conditions compared to dry conditions. It was assumed that the fibrous mats absorbed abundant water and thus reduced the capability of resisting deformation, whereas in dry conditions there existed a high sliding frictional resistance between polymer chains [71].

The strain-to-failure of the scaffolds significantly dropped from $372\% \pm 25\%$ for PGS fibers to $25\% \pm 13\%$ for PGS/PANI blend fibers with PANI content of 2.4% (w/v) in dry condition. Besides, the strain-to-failure of the PGS/PANI scaffolds decreased from $247\% \pm 21\%$ to $44\% \pm 8\%$ in water bath at 37 °C. It can be concluded that the fibrous sheets became less elastic when added more PANI. But the strain-to-failure ranges of the PGS/PANI scaffolds are still enough for cardiac tissue engineering, since the cyclic physiological strain of the natural cardiac tissue is between 5 and 10% during the cardiac cycle [11].

Furthermore, it was observed that the aligned scaffolds in PD direction were stiffer compared to XD direction, which led to anisotropic features for aligned scaffolds. As shown in Fig. 5g, the aligned 2.4% (w/v) PGS/PANI scaffolds presented the highest anisotropic characteristics. Their elastic modulus and UTS in PD direction was respectively almost 5 and 4 times that in XD direction. Moreover, the elastic modulus and UTS of the aligned scaffolds in PD direction were also higher than random scaffolds no matter in dry condition or in wet condition. For instance, the elastic modulus of the aligned 1.6% (w/v) PGS/PANI scaffolds in PD direction was 10.72 ± 0.77 MPa (dry condition) and 3.43 ± 1.44 MPa (wet condition), while that of the random 1.6% (w/v) PGS/PVA/PANI scaffolds was 4.79 ± 0.49 MPa (dry condition) and 2.16 ± 0.69 MPa (wet condition). This might be owing to the inherent structural characteristics of aligned fibers that they could orient along the tensile stress direction and underwent fast fiber rearrangement process at initial tensile stresses [72]. Thus, the aligned PGS/PANI scaffolds were able to bear a higher load compared to the random scaffolds. In order to evaluate the effect of fiber orientation on mechanical properties, the morphology of fractural interface of typical random and aligned 2% (w/v) PGS/PANI scaffolds after uniaxial tensile testing was conducted by SEM. As shown in Fig. 5h–j, in random scaffolds, the intertwined fibers evenly distributed and formed porous structure, at the same time,

fibers randomly ruptured under the tensile stresses. As expected, most aligned scaffolds in XD direction seemed to fracture at the gaps of the adjacent paralleled fibers. Different from XD direction, the fracture of most fibers occurred and caused the whole breakage of the aligned scaffolds in PD direction. From the analysis of these fracture morphologies for different kinds of scaffolds, it is understandable that aligned fibrous mats in PD direction were inclined to show the highest mechanical strength.

As is well known, to mimic the constant beating behavior of the myocardium, the scaffolds applied in cardiac tissue engineering are supposed to possess fatigue resistance property. Therefore, the random and aligned 1.6% (w/v) PGS/PANI fibrous membranes in both PD and XD directions were cyclically stretched for 50 cycles at room temperature. As illustrated in Fig. 6a–c, All of PGS/PANI fibrous scaffolds showed an obvious hysteresis loop in the first cycle. With the increasing of cycle numbers, the hysteresis loops became smaller and closer. During the first 20 cycles of a dynamic tensile test, the PGS/PANI seemed to behave as a viscoelastic material. After 20 cycles, the curves of all PGS/PANI scaffolds almost entirely overlapped. Although there existing irreversible deformation at initial cycles which might be caused by the plasticity deformation of the hard components like stiff and brittle PANI, the scaffolds were still capable of undergoing reversible deformations under a dynamic cyclic tensile test, indicating its elastic properties and potential application in myocardial regeneration.

3.8. Degradation behavior

The in vitro degradation behavior of the PGS/PANI scaffolds with different PANI concentration was assessed by immersing in lipase enzymatic solution at 37 °C for 16 days. Additionally, mass losses of degraded samples were acquired and compared with those of the non-degraded samples (Fig. 4c). The weight loss of the PGS and PGS/PANI scaffolds (1.2% (w/v), 1.6% (w/v), 2% (w/v) and 2.4% (w/v)) reached $68\% \pm 1.77\%$, $26.87\% \pm 1.08\%$, $17.3\% \pm 8.78\%$, $20.07\% \pm 3.83\%$, and $6.17\% \pm 1.02\%$ after 16 days of the incubation, respectively. PGS fibrous mats exhibited nearly linear degradation profile and the highest weight loss compared to PGS/PANI scaffolds. The reason for the fast degradation rate of PGS scaffolds may be that the lipase enzyme could catalyze the hydrolysis of the ester bonds in PGS blends. And the H^+ release induced autocatalytic effect. As the PANI content increased, the degradation rate of PGS/PANI scaffolds significantly decreased, this phenomenon might be attributed to that the addition of PANI induced a buffering effect, which alleviated a localized acidic environment created by the acidic degradation products of PGS [28]. Because of the intrinsic strength of PANI, the stability of the composite PGS/PANI scaffolds was enhanced. This kind of slow degradation rate was favorable for cardiac tissue engineering because it could provide a suitable substrate for long-term cardiomyocyte growth.

Fig. S6 presented SEM micrographs of PGS/PANI scaffolds with different PANI content after 1, 2, 6, 10 and 16 days in enzyme solution, respectively. Before degradation, the PGS fibers fused into an intact film without fibrous structure. Although PGS scaffolds showed obvious mass loss, there was absence of morphological changes with increasing incubation time, in other words, the film morphology without holes and cracks were still remained, indicating its surface degradation mechanism. The relatively low weight loss of PGS/PANI fibrous scaffolds after 16 days was confirmed by SEM observation. It has been verified that PANI was a non-biodegradable polymer due to the absence of cleavable moieties [54]. The fibrous sheets didn't demonstrate significant morphological changes after 16 days compared to day 1, and it was notable that fibrous topographical features along with scattered PANI particles were still maintained. The stable fibrous structure of PGS/PANI scaffolds made their application in cardiac tissue engineering considerable.

To investigate the degradation behavior that more applicable and reliable to human, the PGS/PANI scaffolds with different PANI content
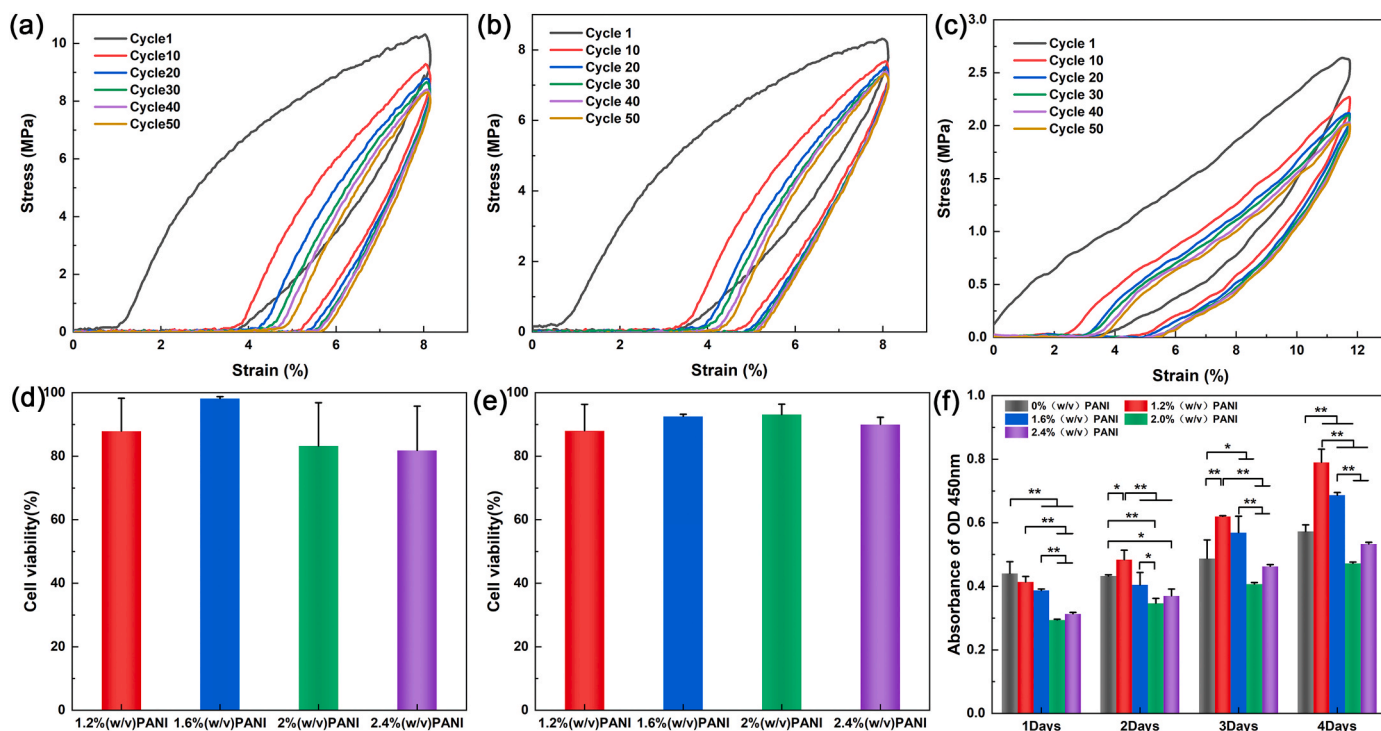
Fig. 6. (a) Hysteresis loops of random PGS/PANI fibrous scaffolds under a 50-cyclic tensile test. (b) Hysteresis loops of aligned PGS/PANI fibrous scaffolds in PD direction under a 50-cyclic tensile test. (c) Hysteresis loops of aligned PGS/PANI fibrous scaffolds in XD direction under a 50-cyclic tensile test. (d) Quantified results of live/dead assay for H9c2 cells seeded on random PGS/PANI scaffolds with different PANI concentrations. (e) Quantified results of live/dead assay for H9c2 cells seeded on aligned PGS/PANI scaffolds with different PANI concentrations. (f) CCK-8 assay of H9c2 cells proliferation on the aligned electrospun fibrous mats after 1, 2, 3 and 4 days of incubation ($n \geq 3$, *$P < 0.05$).

were subcutaneously implanted into the classical animal model rats in vivo. SEM analysis was used to assay the morphological changes of these scaffolds that were harvested for 2, 4, 6 and 8 weeks (Figs. S7 and S8). In contrast to the exhibition of smooth appearance of fibers before degradation, PGS/PANI scaffolds showed an increased surface roughness along with the degradation proceeding. It was found that some tissues and cells migrated into porous fibrous sheets and spaces between layers of fibrous mats. After 4 weeks, some fibers of the PGS/PANI scaffolds were fused and swollen. The PANI particles were still remained within the fibers. When compared with in vitro degradation, the subcutaneous implantation of fibrous PGS/PANI mats showed a significantly higher degradation rate because the infiltration of tissues into fibrous scaffolds destroyed the structural integrity resulted in the disappearance of some fibers.

3.9. Cell viability, adhesion and proliferation of H9c2 cells on nanofibrous sheets

To evaluate whether these PGS/PANI fibrous scaffolds with different PANI contents could be used in cardiac tissue engineering, the biocompatibility of these scaffolds was characterized by utilizing H9c2 cells, because this kind of rat cardiomyocyte cell line has been extensively introduced as a useful model system for verifying the ability of biomaterials to support cardiac cells proliferation [63,73,74]. H9c2 cells were seeded on the surface of the PGS/PANI scaffolds for 24 h and the cell viability was assessed by live/dead staining. The green fluorescence signified the living cells, and the red fluorescence represented the dead cells. As shown in Fig. 7a and b, the majority of H9c2 cells on all PGS/PANI scaffolds showed green fluorescence which suggested good cell compatibility of the PGS/PANI scaffolds. Additionally, the alignment of the H9c2 cells along the fiber direction of each aligned scaffold was evident, indicating the aligned fibrous PGS/PANI scaffolds could support cell orientation by affording well defined topographical cues. It

was inspiring for this result because cardiomyocytes alignment was vital for the formation of organized sarcomeres. The quantitative analysis of the cell viability on random and aligned PGS/PANI scaffolds (1.2% (w/v), 1.6% (w/v), 2% (w/v) and 2.4% (w/v)) were showed in Fig. 6d and e. It could be observed that 1.6% (w/v) PGS/PANI scaffolds had the highest cell viability among these fibrous scaffolds no matter in random or aligned direction. The viability of H9c2 cells was high at 82%–98% range on these PGS/PANI scaffolds.

The cell proliferation of H9c2 cells on aligned the PGS/PANI fibrous sheets was further carried out by CCK-8 assay during 4 days cultivation Fig. 6f. It was showed that the proliferation of H9C2 cardiomyocytes increased significantly on all samples along with time extension. On the first day of cell culture, highest cell viability was observed for PGS/PVA scaffolds without PANI. However, the number of viable cells cultured on the 1.2% (w/v) PGS/PANI scaffolds was highest than that on the other scaffolds after 2 days incubation. These results indicated that the addition of conductive PANI into PGS scaffolds might improve cells' proliferation and didn't induce obvious cytotoxicity. This outcome was in agreement with the findings of other studies whose prepared scaffolds contained PANI [63,69,75]. For instance, in a recent work, a nanofibrous composite made of collagen, hyaluronic acid and PANI was fabricated by electrospinning and the enhanced expression of connexin 43 as well as longer contraction time indicated the positive effect of PANI on cell proliferations [54]. It has also been proved that many factors such as fiber diameters, surface morphology, hydrophilicity and stiffness might affect the cell proliferation [76].

The cell adhesion and spreading on random and aligned PGS/PANI scaffolds for 3 days were examined with the SEM micrographs acquired from H9c2 cells-seeded scaffolds. As shown in Fig. 7c–f, H9c2 cells appeared to attach well on both random and aligned PGS/PANI scaffolds with different PANI concentration. Compared with flat H9c2 cells grown on random fibrous PGS/PANI scaffolds, H9c2 cells grown on aligned PGS/PANI scaffolds tended to organize and elongate along the fiber
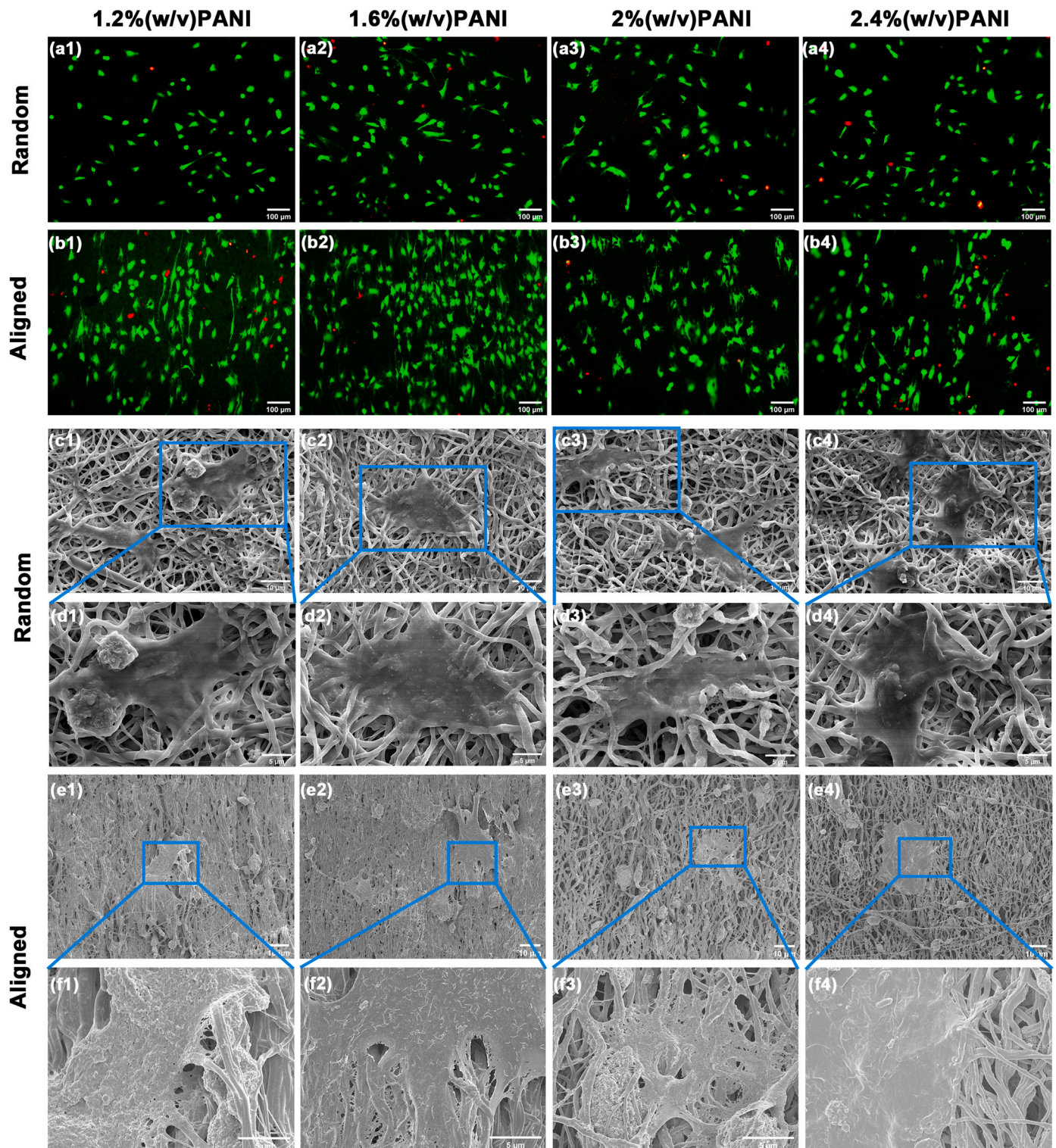
Fig. 7. (a, b) The cell viability of H9c2 cells on random and PGS/PANI scaffolds with 1.2% (w/v) PANI, 1.6% (w/v) PANI, 2% (w/v) PANI and 2.4% (w/v) PANI after seeding for 24 h. (c, d) SEM images related to the H9c2 cells attachment on the random scaffolds after culturing for 3 days (5000× and 10,000× magnification). (e, f) SEM micrographs of cell adhesion on aligned PGS/PANI scaffolds containing different content of PANI particles up to 3 days (1000× and 5000× magnification).

direction. Interestingly, to anchor on the fibers, the H9c2 cells endeavored to grasp the fibers that were remote from the main cell body by developing cellular processes, which eventually increased their dimensions with diameters around 15–30 μm. It could also be observed from Fig. S9 that the flatted H9c2 cells not only spread on the surface of the fibrous sheets, but extended bundles of pseudopodia which attached onto and wrapped around the PGS/PANI fibers. The fiber size of these

pseudopodia was in the range of 15–200 nm. The elongation of filopodia within the cytoskeleton suggested desirable interactions and attachment of H9c2 cells with the fibrous PGS/PANI scaffolds.

3.10. In vivo biocompatibility of the PGS/PANI scaffolds

To investigate the in vivo biocompatibility of PGS/PANI scaffolds

with different PANI content, random and aligned PGS/PVA, 1.2% (w/v), 1.6% (w/v), 2% (w/v) and 2.4% (w/v) PGS/PANI fibrous scaffolds were implanted subcutaneously in Wistar rats for 1, 2, 4, 6 and 8 weeks, respectively. As shown in Figs. S10, S11, 8, S12, H&E staining and Masson's trichrome staining were carried out after samples were harvested following implantation. In the H&E staining, the cytoplasm and extracellular matrix were stained pink, and the cell nuclei were stained purplish blue. The Masson's trichrome which stained muscle fibers red, collagen blue, cytoplasm light red and cell nucleus dark brown to black, was also extensively applied in histology.

The PGS strips were nearly transparent or mild white in the H&E staining images, whereas they could be clearly visualized in blue color after being stained with Masson's trichrome. The PGS scaffolds were inclined to bend and conformable to fit into the tissue envelope after implantation due to its flexibility. With the implantation time increased, the PGS scaffolds presented smaller size and more cell recruitment.

In contrast to PGS films, PGS/PANI scaffolds possessed a more diffuse structure which were confirmed by the optical microscope. The fibrous structure of the PGS/PANI scaffolds could be clearly observed. The PGS fibers with light grey color showed nearly isotropic morphology, while the black PANI particles with diameters 2–50 μm were sprinkled throughout the fibrous scaffolds. All of PGS/PANI scaffolds maintained their integrity after implantation for 1 week. However, with the degradation went on, cracks appeared, visible fiber fragmentations and delamination were also observed on some PGS/PANI fibrous scaffolds, especially after 6 weeks implantation.

As is known to all, successful cell growth inside the scaffolds was an essential prerequisite for tissue engineering. The histological sections of the PGS/PANI composite scaffolds revealed substantial infiltration and uniform migration of the cells into the interior regions of the fabricated scaffolds due to the porous architecture induced by the fibrous scaffolds irrespective of their alignment. Collagen deposition is prominent in the blue regions of the Masson's trichrome micrographs. The outer margins of each PGS/PANI scaffolds were surrounded by collagen-rich matrix and neutrophils. At the same time, fibroblast like cells were penetrated within the internal fibrous networks of the scaffolds. As degradation time went on, cells permeated more deeply in the PGS/PANI scaffolds with different PANI content. In 8 weeks following scaffolds implantation, the collagen secreted by the infiltrated cells also emerged in the interior of the scaffolds. It could also be noticed that some blood vessels formed around the fibrous scaffolds, which were important to provide nutrients for surrounding cells and transfer away metabolic wastes [77]. Cell infiltration plays a crucial role in the formation of cell-scaffold construct. Both the physicochemical properties of scaffold materials and microarchitecture of scaffolds strongly influence the cell infiltration in vivo. For example, it has been reported that hydrophobic nature of most synthetic scaffold polymers is not advantageous for cells adhesion and subsequent infiltration because of unsatisfactory wettability [78].
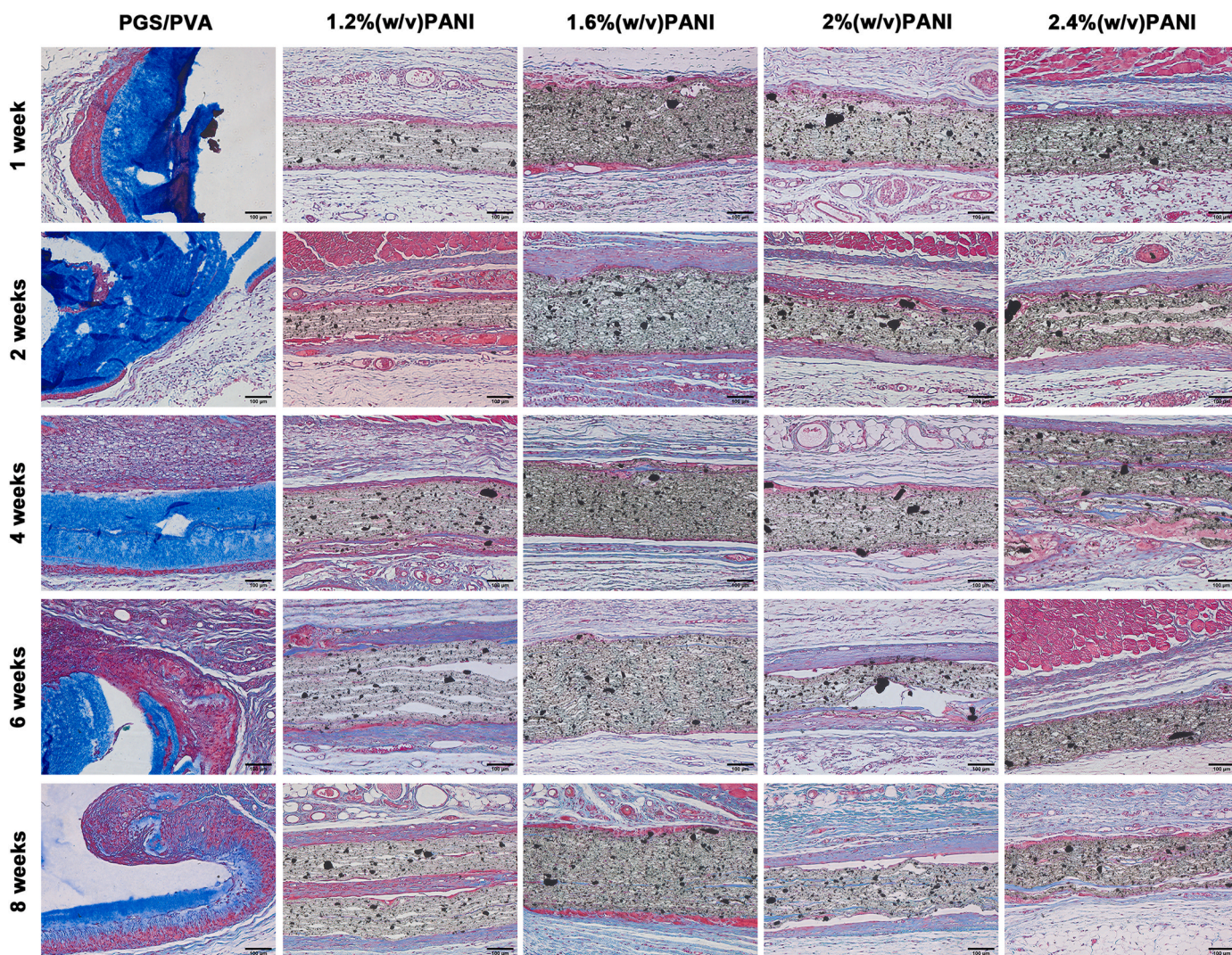

Fig. 8. Representative Masson's trichrome staining images of random fibrous PGS scaffolds with 0% (w/v) PANI, 1.2% (w/v) PANI, 1.6% (w/v) PANI, 2% (w/v) PANI and 2.4% (w/v) PANI after implantation for 1, 2, 4, 6 and 8 weeks.

To overcome this drawback, a combination of hydrophilic natural polymers with synthetic polymers and surface modification like functionalization with polydopamine (pDA) and heparin coating have been proposed [79–81]. It has been suggested that the mechanical performance of the scaffolds also affect the cell infiltration [82]. Compare to a stiff scaffold, cells migrated more faster in a soft scaffold [83]. In addition to the optimization of scaffold materials, enhanced cell infiltration can be attained by increasing pore size and porosity which are dependent on the fiber diameters [84]. Although the distribution of PANI particles decreased the hydrophilicity of PGS/PANI scaffolds, the cells could infiltrate deeply into the interior of the scaffolds due to their porous structure and elastic properties.

The rats in random 2.4% (w/v) PGS/PANI groups produced thinner fiber connective tissue than the groups of other scaffolds with different PANI content, indicating better biocompatibility. The thickness of the connective tissue in Wistar rats was thinnest in the first week implantation. As can be noticed, the thickness of connective tissue in 2 weeks implantation was apparently higher than that in the 1week implantation, there existed significant difference between the two time points. Additionally, it seemed that the connective tissue of 4 weeks was thinner when compared to that of 6 weeks or 8 weeks.

Apart from histological observation of these random blend fibrous scaffolds, aligned PGS/PANI scaffolds with different PANI content were also assessed using H&E staining and Masson's trichrome staining method. As shown in Figs. S11 and S12, it could be observed that there were more fiber delamination and breakage in aligned scaffolds in comparison with random scaffolds since the adopted aligned scaffolds were thinner than random scaffolds. Furthermore, 2.4% (w/v) and 2% (w/v) PGS/PANI fibrous scaffolds could maintain better integrity without obvious fiber segregation, indicating that more PANI particles might serve as barrier to delay the degradation rate of PGS fibers. This phenomenon was also consistent with the mass loss results of the above in vitro degradation test. Additionally, the aligned PGS/PANI scaffolds were also surrounded by fibrous connective tissue and various cells, and cells were able to penetrate deep into these scaffolds through the gaps between PGS/PVA fibers.

Taken together, All PGS/PANI scaffolds demonstrated relatively weak inflammatory response. With prolongation of implantation duration, the inflammatory response decreased. Adding appropriate PANI content to PGS scaffolds had no apparent effect on the inflammatory reaction of these scaffolds in vivo, and their good biocompatibility indicated the potential application of PGS/PANI fibrous mat as a cardiac patch.

4. Conclusions

In summary, a series of random and aligned biocompatible electroactive fibrous scaffolds were successfully fabricated by incorporating elastic PGS, nontoxic water-soluble carrier PVA and conductive particles PANI through four steps without introducing any toxic substances. These PGS/PANI scaffolds after purification demonstrated satisfactory electroactivity, good hemocompatibility, and fatigue resistance and their stiffnesses were sufficient to withstand the dynamic heart beatings. SEM and histological images revealed a homogeneous distribution of PANI particles among the PGS fibers, and thus with the addition of PANI particles, the elastic modulus of the scaffolds was significantly increased, while the strain-to-failure was meaningfully decreased. Meanwhile, the incorporation of PANI significantly reduced degradation rate of the PGS fibrous scaffolds owing to its excellent buffering effect. Whether in the wet or the dry conditions, the aligned scaffolds showed different mechanical behavior in the XD and PD directions which can mimic the anisotropy of the natural myocardium. As it expected, all of random and aligned PGS/PANI blend fibers were capable of supporting adhesion, migration, and proliferation of H9c2 rat cardiac myoblasts. Compared with other groups of PGS/PANI scaffolds with different PANI content, 1.6% (w/v) PGS/PANI fibrous scaffolds had better attachment

and proliferation of the H9c2 cardiomyocyte cell line. Additionally, the aligned fibrous structure of PGS/PANI mats significantly promoted cellular elongation and alignment. Besides, the cell infiltration, collagen deposition and degradation observed in the fibrous PGS/PANI scaffolds proved its good histocompatibility. Therefore, by designing different fibrous structure and altering the composition of the scaffolds, the PGS/PANI scaffolds could mimic the structure of natural cardiac ECM, providing tailorable mechanical properties and electroactivities, and was very suitable for cardiac tissue engineering.

CRediT authorship contribution statement

Zebin Wu: Investigation, Methodology, Data curation, Validation, Formal analysis, Software, Writing – original draft, Writing – review & editing. **Qiao Li:** Methodology, Validation, Writing – review & editing. **Lizhen Wang:** Conceptualization, Resources, Writing – review & editing, Supervision, Funding acquisition. **Yang Zhang:** Methodology. **Wei Liu:** Writing – review & editing. **Shudong Zhao:** Methodology. **Xuezheng Geng:** Methodology. **Yubo Fan:** Conceptualization, Resources, Supervision, Funding acquisition.

Declaration of competing interest

The authors declare that they have no known competing financial interests or personal relationships that could have appeared to influence the work reported in this paper.

Data availability

Data will be made available on request.

Acknowledgements

Appendix A. Supplementary data

Supplementary data to this article can be found online at https://doi.org/10.1016/j.mtbio.2023.100798.

References

[1] E. Tzahor, K.D. Poss, Cardiac regeneration strategies: staying young at heart, Science 356 (2017) 1035–1039.

[2] M. Tajabadi, H. Goran Orimi, M.R. Ramzgouyan, A. Nemati, N. Deravi, N. Beheshtizadeh, M. Azami, Regenerative strategies for the consequences of myocardial infarction: chronological indication and upcoming visions, Biomed. Pharmacother. 146 (2022), 112584.

[3] N. Goonoo, Tunable biomaterials for myocardial tissue regeneration: promising new strategies for advanced biointerface control and improved therapeutic outcomes, Biomater. Sci. 10 (2022) 1626–1646.

[4] Y. Fang, W. Sun, T. Zhang, Z. Xiong, Recent advances on bioengineering approaches for fabrication of functional engineered cardiac pumps: a review, Biomaterials 280 (2022), 121298.

[5] L. Lou, K.O. Lopez, P. Nautiyal, A. Agarwal, Integrated perspective of scaffold designing and multiscale mechanics in cardiac bioengineering, Adv. Nanobiomed. Res. 1 (2021), 2100075.

[6] J. Paez-Mayorga, G. Hernández-Vargas, G.U. Ruiz-Esparza, H.M.N. Iqbal, X. Wang, Y.S. Zhang, R. Parra-Saldivar, A. Khademhosseini, Bioreactors for cardiac tissue engineering, Adv. Healthcare Mater. 8 (2019) 1–14.

[7] S. Mehrotra, R.D. Singh, A. Bandyopadhyay, G. Janani, S. Dey, B.B. Mandal, Engineering microsphere-loaded non-mulberry silk-based 3D bioprinted vascularized cardiac patches with oxygen-releasing and immunomodulatory potential, ACS Appl. Mater. Interfaces 13 (2021) 50744–50759.

[8] W.T. Tung, J.A. Maring, X. Xu, Y. Liu, M. Becker, D.B. Somesh, K. Klose, W. Wang, X. Sun, I. Ullah, K. Kratz, A.T. Neffe, C. Stamm, N. Ma, A. Lendlein, In vivo performance of a cell and factor free multifunctional fiber mesh modulating postinfarct myocardial remodeling, Adv. Funct. Mater. 32 (2022), 2110179.

[9] Z. Chu, Q. Zheng, M. Guo, J. Yao, P. Xu, W. Feng, Y. Hou, G. Zhou, L. Wang, X. Li, Y. Fan, The effect of fluid shear stress on the in vitro degradation of poly(lactide-co-glycolide) acid membranes, J. Biomed. Mater. Res. 104 (2016) 2315–2324.

[10] M. Tamimi, S. Rajabi, M. Pezeshki-Modaress, Cardiac ECM/chitosan/alginate ternary scaffolds for cardiac tissue engineering application, Int. J. Biol. Macromol. 164 (2020) 389–402.

[11] S. Mehrotra, B.A.G. de Melo, M. Hirano, W. Keung, R.A. Li, B.B. Mandal, S.R. Shin, Nonmulberry silk based ink for fabricating mechanically robust cardiac patches and endothelialized myocardium-on-a-chip application, Adv. Funct. Mater. 30 (2020) 1–16.

[12] Y. Liang, A. Mitriashkin, T.T. Lim, J.C.H. Goh, Conductive polypyrrole-encapsulated silk fibroin fibers for cardiac tissue engineering, Biomaterials 276 (2021) 121008.

[13] F. Zhang, M.W. King, Biodegradable polymers as the pivotal player in the design of tissue engineering scaffolds, Adv. Healthcare Mater. 9 (2020), 1901358.

[14] P. Montero, M. Flandes-Iparraguirre, S. Musquiz, M. Pérez Araluce, D. Plano, C. Sanmartín, G. Orive, J.J. Gavira, F. Prosper, M.M. Mazo, Cells, materials, and fabrication processes for cardiac tissue engineering, Front. Bioeng. Biotechnol. 8 (2020) 955.

[15] Y. Wang, G.A. Ameer, B.J. Sheppard, R. Langer, A tough biodegradable elastomer, Nat. Biotechnol. 20 (2002) 602–606.

[16] Z. Wu, K. Jin, L. Wang, Y. Fan, A review: optimization for poly(glycerol sebacate) and fabrication techniques for its centered scaffolds, Macromol. Biosci. 21 (2021), 2100022.

[17] S. Chen, Z. Wu, C. Chu, Y. Ni, R.E. Neisiany, Z. You, Biodegradable elastomers and gels for elastic electronics, Adv. Sci. 9 (2022), 2105146.

[18] G.C. Engelmayr, M. Cheng, C.J. Bettinger, J.T. Borenstein, R. Langer, L.E. Freed, Accordion-like honeycombs for tissue engineering of cardiac anisotropy, Nat. Mater. 7 (2008) 1003–1010.

[19] M. Shi, L. Bai, M. Xu, Z. Li, T. Hu, J. Hu, Z. Zhang, Z. Yin, B. Guo, Micropatterned conductive elastomer patch based on poly(glycerol sebacate)-graphene for cardiac tissue repair, Biofabrication 14 (2022), 035001.

[20] M. Morsink, P. Severino, E. Luna-Ceron, M.A. Hussain, N. Sobahi, S.R. Shin, Effects of electrically conductive nano-biomaterials on regulating cardiomyocyte behavior for cardiac repair and regeneration, Acta Biomater. 139 (2022) 141–156.

[21] K. Ashtari, H. Nazari, H. Ko, P. Tebon, M. Akhshik, M. Akbari, S.N. Alhosseini, M. Mozafari, B. Mehravi, M. Soleimani, R. Ardehali, M. Ebrahimi Warkiani, S. Ahadian, A. Khademhosseini, Electrically conductive nanomaterials for cardiac tissue engineering, Adv. Drug Deliv. Rev. 144 (2019) 162–179.

[22] H. Esmaeili, A. Patino-Guerrero, M. Hasany, M.O. Ansari, A. Memic, A. Dolatshahi-Pirouz, M. Nikkhah, Electroconductive biomaterials for cardiac tissue engineering, Acta Biomater. 139 (2022) 118–140.

[23] R. Dong, P.X. Ma, B. Guo, Conductive biomaterials for muscle tissue engineering, Biomaterials 229 (2020), 119584.

[24] B. Guo, P.X. Ma, Conducting polymers for tissue engineering, Biomacromolecules 19 (2018) 1764–1782.

[25] M. Ghovvati, M. Kharaziha, R. Ardehali, N. Annabi, Recent advances in designing electroconductive biomaterials for cardiac tissue engineering, Adv. Healthcare Mater. 11 (2022), 2200055.

[26] Y. Li, L. Wei, L. Lan, Y. Gao, Q. Zhang, H. Dawit, J. Mao, L. Guo, L. Shen, L. Wang, Conductive biomaterials for cardiac repair: a review, Acta Biomater. 139 (2022) 157–178.

[27] K. Nawaka, C. Putson, Enhanced electric field induced strain in electrostrictive polyurethane composites fibers with polyaniline (emeraldine salt) spider-web network, Compos. Sci. Technol. 198 (2020), 108293.

[28] T.H. Qazi, R. Rai, D. Dippold, J.E. Roether, D.W. Schubert, E. Rosellini, N. Barbani, A.R. Boccaccini, Development and characterization of novel electrically conductive PANI-PGS composites for cardiac tissue engineering applications, Acta Biomater. 10 (2014) 2434–2445.

[29] S. Ostrovidov, M. Ebrahimi, H. Bae, H.K. Nguyen, S. Salehi, S.B. Kim, A. Kumatani, T. Matsue, X. Shi, K. Nakajima, S. Hidema, M. Osanai, A. Khademhosseini, Gelatin-polyaniline composite nanofibers enhanced excitation-contraction coupling system maturation in myotubes, ACS Appl. Mater. Interfaces 9 (2017) 42444–42458.

[30] J. Feng, H. Shi, X. Yang, S. Xiao, Self-adhesion conductive sub-micron fiber cardiac patch from shape memory polymers to promote electrical signal transduction function, ACS Appl. Mater. Interfaces 13 (2021) 19593–19602.

[31] M.F. Tenreiro, A.F. Louro, P.M. Alves, M. Serra, Next generation of heart regenerative therapies: progress and promise of cardiac tissue engineering, NPJ Regen. Med. 6 (2021) 1–17.

[32] K.D. Dwyer, K.L.K. Coulombe, Cardiac mechanostructure: using mechanics and anisotropy as inspiration for developing epicardial therapies in treating myocardial infarction, Bioact. Mater. 6 (2021) 2198–2220.

[33] J. Xue, T. Wu, Y. Dai, Y. Xia, Electrospinning and electrospun nanofibers: methods, materials, and applications, Chem. Rev. 119 (2019) 5298–5415.

[34] S. Shi, Y. Si, Y. Han, T. Wu, M.I. Iqbal, B. Fei, R.K.Y. Li, J. Hu, J. Qu, Recent progress in protective membranes fabricated via electrospinning: advanced materials, biomimetic structures, and functional applications, Adv. Mater. 34 (2022) 1–31.

[35] R. Liu, L. Hou, G. Yue, H. Li, J. Zhang, J. Liu, B. Miao, N. Wang, J. Bai, Z. Cui, T. Liu, Y. Zhao, Progress of fabrication and applications of electrospun hierarchically porous nanofibers, Adv. Fiber Mater. 4 (2022) 604–630.

[36] E.M. Jeffries, R.A. Allen, J. Gao, M. Pesce, Y. Wang, Highly elastic and suturable electrospun poly(glycerol sebacate) fibrous scaffolds, Acta Biomater. 18 (2015) 30–39.

[37] L. Vogt, F. Ruther, S. Salehi, A.R. Boccaccini, Poly(Glycerol sebacate) in biomedical applications—a review of the recent literature, Adv. Healthcare Mater. 10 (2021), 2002026.

[38] W. Chen, W. Xiao, X. Liu, P. Yuan, S. Zhang, Y. Wang, W. Wu, Pharmacological manipulation of macrophage autophagy effectively rejuvenates the regenerative potential of biodegrading vascular graft in aging body, Bioact. Mater. 11 (2022) 283–299.

[39] I. Apsite, G. Constante, M. Dulle, L. Vogt, A. Caspari, A.R. Boccaccini, A. Synytska, S. Salehi, L. Ionov, 4D Biofabrication of fibrous artificial nerve graft for neuron regeneration, Biofabrication 12 (2020), 035027.

[40] D. Sha, Z. Wu, J. Zhang, Y. Ma, Z. Yang, Y. Yuan, Development of modified and multifunctional poly(glycerol sebacate) (PGS)-based biomaterials for biomedical applications, Eur. Polym. J. 161 (2021), 110830.

[41] A. Saudi, S. Amini, N. Amirpour, M. Kazemi, A. Zargar Kharazi, H. Salehi, M. Rafienia, Promoting neural cell proliferation and differentiation by incorporating lignin into electrospun poly(vinyl alcohol) and poly(glycerol sebacate) fibers, Mater. Sci. Eng. C 104 (2019), 110005.

[42] L. Jiang, Y. Jiang, J. Stiadle, X. Wang, L. Wang, Q. Li, C. Shen, S.L. Thibeault, L. S. Turng, Electrospun nanofibrous thermoplastic polyurethane/poly(glycerol sebacate) hybrid scaffolds for vocal fold tissue engineering applications, Mater. Sci. Eng. C 94 (2019) 740–749.

[43] M. Teodorescu, M. Bercea, S. Morariu, Biomaterials of PVA and PVP in medical and pharmaceutical applications: perspectives and challenges, Biotechnol. Adv. 37 (2019) 109–131.

[44] A. Saudi, M. Rafienia, A. Zargar Kharazi, H. Salehi, A. Zarrabi, M. Karevan, Design and fabrication of poly(glycerol sebacate)-based fibers for neural tissue engineering: synthesis, electrospinning, and characterization, Polym. Adv. Technol. 30 (2019) 1427–1440.

[45] A. Baji, Y.W. Mai, S.C. Wong, M. Abtahi, P. Chen, Electrospinning of polymer nanofibers: effects on oriented morphology, structures and tensile properties, Compos. Sci. Technol. 70 (2010) 703–718.

[46] G. Yang, X. Li, Y. He, J. Ma, G. Ni, S. Zhou, From nano to micro to macro: electrospun hierarchically structured polymeric fibers for biomedical applications, Prog. Polym. Sci. 81 (2018) 80–113.

[47] A. Abedi, B. Bakhshandeh, A. Babaie, J. Mohammadnejad, S. Vahdat, R. Mombeiny, S.R. Moosavi, J. Amini, L. Tayebi, Concurrent application of conductive biopolymeric chitosan/polyvinyl alcohol/MWCNTs nanofibers, intracellular signaling manipulating molecules and electrical stimulation for more effective cardiac tissue engineering, Mater. Chem. Phys. 258 (2021), 123842.

[48] M. Rekabgardan, A. Parandakh, S. Shahriari, Z.K. Koohpar, M. Rahmani, C. Ganjouri, R.R. Sarbandi, M.M. Khani, An electrospun PGS/PU fibrous scaffold to support and promote endothelial differentiation of mesenchymal stem cells under dynamic culture condition, J. Drug Delivery Sci. Technol. 72 (2022), 103383.

[49] A. Keirouz, G. Fortunato, M. Zhang, A. Callanan, N. Radacsi, Nozzle-free electrospinning of Polyvinylpyrrolidone/Poly(glycerol sebacate) fibrous scaffolds for skin tissue engineering applications, Med. Eng. Phys. 71 (2019) 56–67.

[50] Y. Yan, V. Sencadas, T. Jin, X. Huang, J. Chen, D. Wei, Z. Jiang, Tailoring the wettability and mechanical properties of electrospun poly(L-lactic acid)-poly (glycerol sebacate) core-shell membranes for biomedical applications, J. Colloid Interface Sci. 508 (2017) 87–94.

[51] S. Behtaj, F. Karamali, S. Najafian, E. Masaeli, M.H.N. Esfahani, M. Rybachuk, The role of PGS/PCL scaffolds in promoting differentiation of human embryonic stem cells into retinal ganglion cells, Acta Biomater. 126 (2021) 238–248.

[52] Z. Wu, K. Jin, L. Wang, Y. Fan, Effect of curing time on the mechanical properties of poly (glycerol sebacate), J. Appl. Polym. Sci. (2023), e53700.

[53] Z. Daraeinejad, I. Shabani, Enhancing biocompatibility of polyaniline-based scaffolds by using a bioactive dopant, Synth. Met. 271 (2021), 116642.

[54] K. Roshanbinfar, L. Vogt, F. Ruther, J.A. Roether, A.R. Boccaccini, F.B. Engel, Nanofibrous composite with tailorable electrical and mechanical properties for cardiac tissue engineering, Adv. Funct. Mater. 30 (2020), 1908612.

[55] L. Yu, G. Zeng, J. Xu, M. Han, Z. Wang, T. Li, M. Long, L. Wang, W. Huang, Y. Wu, Development of poly(glycerol sebacate) and its derivatives: a review of the progress over the past two decades, Polym. Rev. (2022) 1–66.

[56] M. Rostamian, H. Hosseini, V. Fakhri, P.Y. Talouki, M. Farahani, A.J. Gharehtzpeh, V. Goodarzi, C.H. Su, Introducing a bio sorbent for removal of methylene blue dye based on flexible poly(glycerol sebacate)/chitosan/graphene oxide ecofriendly nanocomposites, Chemosphere 289 (2022), 133219.

[57] D. Qureshi, A. Sahoo, B. Mohanty, A. Anis, V. Kulikouskaya, K. Hileuskaya, V. Agabekov, P. Sarkar, S.S. Ray, S. Maji, K. Pal, Fabrication and characterization of poly (Vinyl alcohol) and chitosan oligosaccharide-based blend films, Gels 7 (2021) 1–23.

[58] A. Angelini, A. Car, I.A. Dinu, L. Leva, W. Yave, Amphiphilic poly(vinyl alcohol) membranes leaving out chemical cross-linkers: design, synthesis, and function of tailor-made poly(vinyl alcohol)-b-poly(styrene) copolymers, Macromol. Rapid Commun. (2023), 2200875, 1–12.

[59] S. Rastegar, M. Mehdikhani, A. Bigham, E. Poorazizi, M. Rafienia, Poly glycerol sebacate/polycaprolactone/carbon quantum dots fibrous scaffold as a multifunctional platform for cardiac tissue engineering, Mater. Chem. Phys. 266 (2021), 124543.

[60] Y. Yin, J. Mo, J. Feng, Conductive fabric patch with controllable porous structure and elastic properties for tissue engineering applications, J. Mater. Sci. 55 (2020) 17120–17133.

[61] E.N. Zare, P. Makvandi, B. Ashtari, F. Rossi, A. Motahari, G. Perale, Progress in conductive polyaniline-based nanocomposites for biomedical applications: a review, J. Med. Chem. 63 (2020) 1–22.

[62] S. Kopyl, R. Surmenev, M. Surmeneva, Y. Fetisov, A. Kholkin, Magnetoelectric effect: principles and applications in biology and medicine– a review, Mater. Today Bio 12 (2021).

[63] L. Wang, Y. Wu, T. Hu, B. Guo, P.X. Ma, Electrospun conductive nanofibrous scaffolds for engineering cardiac tissue and 3D bioactuators, Acta Biomater. 59 (2017) 68–81.

[64] M. Li, J. Chen, M. Shi, H. Zhang, P.X. Ma, B. Guo, Electroactive anti-oxidant polyurethane elastomers with shape memory property as non-adherent wound dressing to enhance wound healing, Chem. Eng. J. 375 (2019), 121999.

[65] D. Mawad, C. Mansfield, A. Lauto, F. Perbellini, G.W. Nelson, J. Tonkin, S.O. Bello, D.J. Carrad, A.P. Micolich, M.M. Mahat, J. Furman, D.J. Payne, A.R. Lyon, J. J. Gooding, S.E. Harding, C.M. Terracciano, M.M. Stevens, A Conducting polymer with enhanced electronic stability applied in cardiac models, Sci. Adv. 2 (2016), e1601007.

[66] D. Motlagh, J. Yang, K.Y. Lui, A.R. Webb, G.A. Ameer, Hemocompatibility evaluation of poly(glycerol-sebacate) in vitro for vascular tissue engineering, Biomaterials 27 (2006) 4315–4324.

[67] S. Kouser, S. Sheik, G.K. Nagaraja, A. Prabhu, K. Prashantha, J.N. D'souza, K. M. Navada, D.J. Manasa, Functionalization of halloysite nanotube with chitosan reinforced poly (vinyl alcohol) nanocomposites for potential biomedical applications, Int. J. Biol. Macromol. 165 (2020) 1079–1092.

[68] M. Li, Y. Guo, Y. Wei, A.G. MacDiarmid, P.I. Lelkes, Electrospinning polyaniline-contained gelatin nanofibers for tissue engineering applications, Biomaterials 27 (2006) 2705–2715.

[69] M.C. Chen, Y.C. Sun, Y.H. Chen, Electrically conductive nanofibers with highly oriented structures and their potential application in skeletal muscle tissue engineering, Acta Biomater. 9 (2013) 5562–5572.

[70] S.I. Jeong, I.D. Jun, M.J. Choi, Y.C. Nho, Y.M. Lee, H. Shin, Development of electroactive and elastic nanofibers that contain polyaniline and poly(L-lactide-co-ε-caprolactone) for the control of cell adhesion, Macromol. Biosci. 8 (2008) 627–637.

[71] N. Masoumi, B.L. Larson, N. Annabi, M. Kharaziha, B. Zamanian, K.S. Shapero, A. T. Cubberley, G. Camci-Unal, K.B. Manning, J.E. Mayer, A. Khademhosseini, P.G. S. Electrospun, PCL microfibers align human valvular interstitial cells and provide tunable scaffold anisotropy, Adv. Healthcare Mater. 3 (2014) 929–939.

[72] A.K. Gaharwar, M. Nikkhah, S. Sant, A. Khademhosseini, Anisotropic poly(glycerol sebacate)-poly (-caprolactone) electrospun fibers promote endothelial cell guidance, Biofabrication 7 (2015), 15001.

[73] Y. Yao, J. Ding, Z. Wang, H. Zhang, J. Xie, Y. Wang, L. Hong, Z. Mao, J. Gao, C. Gao, ROS-responsive polyurethane fibrous patches loaded with methylprednisolone (MP) for restoring structures and functions of infarcted myocardium in vivo, Biomaterials 232 (2020), 119726.

[74] T. Hu, Y. Wu, X. Zhao, L. Wang, L. Bi, P.X. Ma, B. Guo, Micropatterned, electroactive, and biodegradable poly(glycerol sebacate)-aniline trimer elastomer for cardiac tissue engineering, Chem. Eng. J. 366 (2019) 208–222.

[75] C.W. Hsiao, M.Y. Bai, Y. Chang, M.F. Chung, T.Y. Lee, C.T. Wu, B. Maiti, Z.X. Liao, R.K. Li, H.W. Sung, Electrical coupling of isolated cardiomyocyte clusters grown on aligned conductive nanofibrous meshes for their synchronized beating, Biomaterials 34 (2013) 1063–1072.

[76] A. Saudi, S.M. Zebarjad, H. Alipour, E. Katoueizadeh, A. Alizadeh, M. Rafienia, A study on the role of multi-walled carbon nanotubes on the properties of electrospun Poly(Caprolactone)/Poly(Glycerol sebacate) scaffold for nerve tissue applications, Mater. Chem. Phys. 282 (2022), 125868.

[77] K. Li, Y. Zhang, J. Xu, J. Wang, X. Gu, P. Li, Y. Fan, Three-dimensional magnetic fibrous scaffold with icariin expanded by supercritical CO2 for bone tissue engineering under static magnetic field, Compos. B Eng. 226 (2021), 109304.

[78] M. Kharaziha, M.H. Fathi, H. Edris, Tunable cellular interactions and physical properties of nanofibrous PCL-forsterite: gelatin scaffold through sequential electrospinning, Compos. Sci. Technol. 87 (2013) 182–188.

[79] M.B. Taskin, R. Xu, H. Gregersen, J.V. Nygaard, F. Besenbacher, M. Chen, Three-Dimensional polydopamine functionalized coiled microfibrous scaffolds enhance human mesenchymal stem cells colonization and mild myofibroblastic differentiation, ACS Appl. Mater. Interfaces 8 (2016) 15864–15873.

[80] L. Huang, J. Huang, H. Shao, X. Hu, C. Cao, S. Fan, L. Song, Y. Zhang, Silk scaffolds with gradient pore structure and improved cell infiltration performance, Mater. Sci. Eng. C 94 (2019) 179–189.

[81] K.T. Kurpinski, J.T. Stephenson, R.R.R. Janairo, H. Lee, S. Li, The effect of fiber alignment and heparin coating on cell infiltration into nanofibrous PLLA scaffolds, Biomaterials 31 (2010) 3536–3542.

[82] X. Zhao, X. Sun, L. Yildirimer, Q. Lang, Z.Y. William, R. Lin, Zheng, Y. Zhang, W. Cui, N. Annabi, A. Khademhosseini, Cell infiltrative hydrogel fibrous scaffolds for accelerated wound healing, Acta Biomater. 49 (2017) 66–77.

[83] P. Soman, J.A. Kelber, J.W. Lee, T.N. Wright, K.S. Vecchio, R.L. Klemke, S. Chen, Cancer cell migration within 3D layer-by-layer microfabricated photocrosslinked PEG scaffolds with tunable stiffness, Biomaterials 33 (2012) 7064–7070.

[84] J. Wu, Y. Hong, Enhancing cell infiltration of electrospun fibrous scaffolds in tissue regeneration, Bioact. Mater. 1 (2016) 56–64.